

15 ~~Brownian Dynamics: A Powerful Computational Tool for Ion Permeation in Bio-Nanotubes~~¹

Shin-Ho Chung and Vikram Krishnamurthy

15.1 Introduction

All living cells are surrounded by a thin membrane, composed of two layers of phospholipid molecules, called the lipid bilayer. This thin membrane effectively confines some ions and molecules inside and exchanges others with outside and acts as a hydrophobic, low dielectric barrier to hydrophilic molecules. Because of a large difference between the dielectric constants of the membrane and electrolyte solutions, no charged particles, such as Na^+ , K^+ , and Cl^- ions, can jump across the membrane. The amount of energy needed to transport one monovalent ion, in either direction across the membrane, known as the *Born energy*, is enormously high. For a living cell to function, however, the proper ionic gradient has to be maintained, and ions at times must move across the membrane to maintain the potential difference across the membrane and to generate synaptic and action potentials. The delicate tasks of regulating the transport of ions across the membrane are carried out by biological nanotubes called “ion channels,” water-filled conduits inserted across the cell membrane through which ions can freely move in and out when the gates are open. These ion channels can be viewed as biological sub-nanotubes, the typical pore diameters of which are $\sim 10^{-9}$ m or 10 Å.

Ionic channels in lipid membranes play a crucial role in the existence of living organisms. All electrical activities in the nervous system, including communication between cells and the influence of hormones and drugs on cell function, are regulated by the opening and closing of these membrane proteins. Because these channels are elementary building blocks of brain function, understanding their mechanisms at a molecular level is a fundamental problem in biophysics. Moreover, the elucidation of how single channels work will ultimately help us find the causes of, and potentially cures for, a number of neurological and muscular disorders.

In the past few years, there have been enormous strides in our understanding of the structure–function relationships in biological ion channels. This sudden

¹ This chapter is an extended version of Krishnamurthy and Chung (2005) that appeared in IEEE Transactions Nanobioscience, March 2005.

Shin-Ho Chung and Vikram Krishnamurthy

advance has been brought about by the combined efforts of experimental and computational biophysicists, who together are beginning to unravel the working principles of these exquisitely designed biological nanotubes that regulate the flow of charged particles across living membranes. In recent breakthroughs, the crystal structures of the potassium channels, mechanosensitive channel, chloride channel, and nicotinic acetylcholine receptor have been determined from crystallographic analysis (Doyle et al., 1998; Bass et al., 2002; Dutzler et al., 2002, 2003; Long et al., 2004a,b; Unwin, 2005). It is expected that crystal structures of other ion channels will follow these discoveries, ushering in a new era in ion channel studies, where predicting function of channels from their atomic structures will become the main quest. Parallel to these landmark experimental findings, there have also been important advances in computational biophysics. As new analytical methods have been developed and the available computational power increased, theoretical models of ion permeation have become increasingly sophisticated. Now it has become possible to relate the atomic structure of an ion channel to its function through the fundamental laws of physics operating in electrolyte solutions. Many aspects of macroscopic observable properties of ion channels are being addressed by molecular and stochastic dynamics simulations. Quantitative statements based on rigorous physical laws are replacing qualitative explanations of how ions permeate across narrow pores formed by the protein wall and how ion channels allow one ionic species to pass while blocking others. The computational methods of solving complex biological problems, such as permeation, selectivity and gating mechanisms of ion channels, will increasingly play prominent roles as the speed of computers increases and theoretical approaches that are currently underdevelopment become further refined.

Here we give a brief account of Brownian dynamics (BD), one of the several theoretical computational methods that are being used for treating time-dependent, nonequilibrium processes that underlie the flow of currents across biological ion channels. We first give a simple, intuitive explanation of how one traces the trajectories of ions in electrolyte solutions interacting with a low dielectric boundary. We briefly illustrate how the BD simulation algorithm has been employed in elucidating the mechanisms of ion permeation in the KcsA potassium channel and CIC chloride channels. We then outline the principles underlying BD, its statistical consistency and algorithms for practical implementation. We also describe one novel extension of BD, called adaptive controlled BD simulations, that circumvents some of the caveats to computing current flow across ion channels using the conventional method. Three other computational approaches—the Poisson–Nernst–Planck theory, semi-microscopic Monte Carlo method, and molecular dynamics—are summarized in the preceding and following chapters (Coalson and Kurnikova, 2006; Grottesi et al., 2006; Jordan, 2006). The reader is also referred to recent review articles (Eisenberg, 1999; Partenskii and Jordan, 1992; Roux et al., 2000; Tieleman et al., 2001; Chung and Kuyucak, 2002) for further details of recent advances in ion channel research.

15. Brownian Dynamics

15.2 Stochastic Dynamics Simulations

15.2.1 Overview

One of the ultimate aims of theoretical biophysicists is to provide a comprehensive physical description of biological ion channels. Such a theoretical model, once successfully formulated, will link channel structure to channel function through the fundamental processes operating in electrolyte solutions. It will also concisely summarize the data, by interlacing all those seemingly unrelated and disparate observations into a connected whole. The theory will elucidate the detailed mechanisms of ion permeation—where the binding sites are in the channel, how fast an ion moves from one binding site to another, and where the rate-limiting steps are in conduction. Finally, it will make predictions that can be confirmed or refuted experimentally.

The tools of physics employed in this endeavor, from fundamental to phenomenological, are *ab initio* and classical molecular dynamics, BD, and continuum theories. These approaches make various levels of abstractions in replacing the complex reality with a model, the system composed of channel macromolecules, lipid bilayer, ions, and water molecules. One of the important criteria of successful modeling is that macroscopic observables remain invariant when the real system is replaced by the model. Each of these approaches has its strengths and limitations, and involves a degree of approximation.

At the lowest level of abstraction we have the *ab initio* quantum mechanical approach, in which the interactions between the atoms are determined from first-principle electronic structure calculations. As there are no free parameters in this approach, it represents the ultimate approach to the modeling of biomolecular systems. But because of the extremely demanding nature of computations, its applications are limited to very small systems at present. A higher level of modeling abstraction is to use classical molecular dynamics (Grottesi et al., 2005, 2006). Here, simulations are carried out using empirically-determined pairwise interaction potentials between the atoms, and their trajectories are followed using Newton's equation of motion. Although it is possible to model an entire ion channel in this way, it is not feasible to simulate the system long enough to see permeation of ions across a model channel and to determine its conductance, which is the most important channel property.

For that purpose, one has to go up one further step in abstraction to stochastic dynamics, of which BD is the simplest form, where water molecules that form the bulk of the system in ion channels are integrated out and only the ions themselves are explicitly simulated. Thus, instead of considering the dynamics of individual water molecules, one considers their average effect as a random force or Brownian motion on the ions. This treatment of water molecules can be viewed as a functional central limit theorem approximation. In BD, it is further assumed that the protein is rigid and its dynamics are not considered. Thus, in this approach, the motion of each individual ion is modeled as the evolution of a stochastic differential equation, known as the Langevin equation.

Shin-Ho Chung and Vikram Krishnamurthy

A still higher level of abstraction is the Poisson–Nernst–Planck theory (Coalson and Kurnikova, 2005, 2006), which is based on the continuum hypothesis of electrostatics. In this and other electrodiffusion theories, one makes a further simplification, known as the mean-field approximation. Here, ions are treated not as discrete entities but as continuous charge densities that represent the space–time average of the microscopic motion of ions. In the Poisson–Nernst–Planck theory, the flux of an ionic species is described by the Nernst–Planck equation that combines Ohm’s law with Fick’s law of diffusion, and the potential at each position is determined from the solution of Poisson’s equation using the total charge density (ions plus fixed charges). The Poisson–Nernst–Planck theory thus incorporates the channel structure, and its solution yields the potential, concentration, and flux of ions in the system in a self-consistent manner.

There is one other approach that has been fruitfully employed to model biological ion channels, namely, the reaction rate theory (Jordan, 1999; McCleskey, 1999; Hille, 2001). In this approach, an ion channel is represented by a series of ion binding sites separated by barriers, and ions are assumed to hop from one binding site to another, with the probability of each hop determined by the height of the energy barrier. Although the model parameters have no direct physical relation to the channel structure, many useful insights have been gleaned in the past about the mechanisms of ion permeation using this approach.

15.2.2 General Description of Brownian Dynamics

Brownian dynamics offers one of the simplest methods for following the trajectories of interacting ions in a fluid. Figure 15.1 shows a schematic illustration of a BD simulation assembly. An ion channel representing the potassium channel is placed at the center of the assembly. The positions in three-dimensional space of all the atoms forming the channel are given by its X-ray structure, and the charge on each atom is assigned. Then, a large cylindrical reservoir with a fixed number of K^+ (or Na^+) and Cl^- ions is attached at each end of the channel (Fig. 15.1A) to mimic the extracellular or intracellular space. The membrane potential is imposed by applying a uniform electric field across the channel (Fig. 15.1B). This is equivalent to placing a pair of large plates far away from the channel and applying a potential difference between them. Since the space between the voltage plates is filled with electrolyte solution, each reservoir is in iso-potential. That is, the average potential anywhere in the reservoir is identical to the applied potential at the voltage plate on that side, and the potential drop occurs almost entirely across the channel.

The algorithm for performing BD simulations is conceptually simple. The velocity of the ion with mass m and charge q located at a given position is determined by the force acting on it at time t . This velocity is computed by integrating the equation of motion, known as the Langevin equation. Once its velocity is determined at time t , the position this ion will occupy in three-dimensional space at time $t + \Delta t$ can be specified. The calculation is repeated for each ion in the assembly, and the new distribution of the positions of all ions at time $t + \Delta t$ are assigned. At each

15. Brownian Dynamics

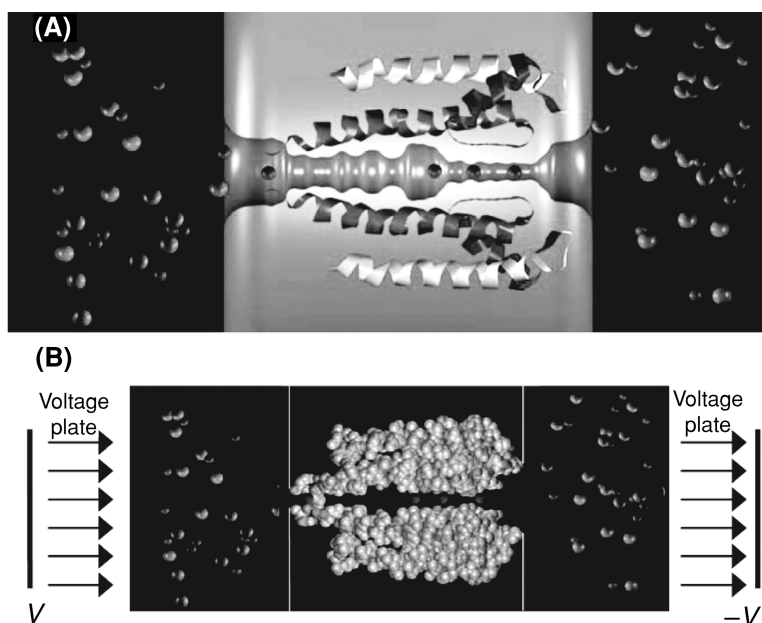


Fig. 15.1 Brownian dynamics setup. (A) The KcsA K^+ channel is placed at the center of the simulation and a large reservoir containing K^+ and Cl^- ions is attached at each end of the protein. The intracellular aspect of the channel is on the left. (B) A uniform electric field is applied across the channel to mimic the membrane potential. This arrangement is equivalent to having two voltage plates far away from the channel.

time-step, usually 2 fs, the forces acting on each ion are calculated and the Langevin equation is used to determine where it will move in the next time-step. By repeating this process many billions of times, usually for a simulation period lasting between 10 and 100 μs , we can trace the movement of each ion in space during a simulation period, and count how many ions have crossed from one side of the channel to the other.

What ultimately determines the motion of ions, and hence the current flowing across the channel, is the total force acting on charged particles. It is important, therefore, to specify all the components of the forces accurately. Two main sources of the forces influencing the motion of ions in or in the vicinity of an ion channel are the “stochastic” force and electric force. The former arises from the effects of collisions between ions and water molecules. Ions in electrolyte solutions are tightly bound by shells of water molecules and these hydrated ions collide incessantly with surrounding water molecules. As a result of such bombardments, the motion of an ion is retarded, and it undergoes random fluctuations from an equilibrium position.

The electric field inside or outside of the channel originates from four different sources. First, there is a field resulting from the membrane potential, which is generated by diffuse, unpaired, ionic clouds on each side of the membrane. Second, there are fixed charges in the channel protein and the electric field emanating from

Shin-Ho Chung and Vikram Krishnamurthy

them adds to the field generated by the membrane potential. Third, charges carried by all the ions in electrolyte solutions contribute to the total electric field. Whenever any of these ions come near the protein wall, it induces surface charges of the same polarity at the water–protein interface. These induced surface charges, the fourth source contributing to the electric field, stem from the fact that polar or carbonyl groups on the protein wall cannot rotate as freely as water molecules. Each of these four components has to be computed and added together to obtain the total electric force experienced by an ion at any given position at any given time. The stochastic force and electrical force acting on a charged particle together determine to which position it will have moved to in a short time interval.

To carry out BD simulations of ion channels, one needs to specify the boundaries of the system. This is a relatively simple problem for one-dimensional BD simulations (Cooper et al., 1985; Jakobsson and Chiu, 1987; Bek and Jakobsson, 1994), but requires the addition of reservoirs to the channel system in the more realistic case of three-dimensional BD simulations. In several recent studies, a simple stochastic boundary has been used successfully in applications of BD simulations to a number of ion channels (Chung et al., 1998, 1999; Corry et al., 2001). When an ion strikes the reservoir boundary during simulations, it is elastically scattered back into the reservoir, equivalent to letting an ion enter the reservoir whenever one leaves the simulation system. Thus the concentrations of ions in the reservoirs are maintained at the desired values at all times. During simulations of current measurements, the chosen concentration values in the reservoirs are maintained by recycling ions from one side to the other whenever there is an imbalance due to a conduction event, mimicking the current flow through a closed circuit.

15.2.3 Two Simplifying Assumption of Brownian Dynamics

The ability to compute current flow across ion channels confers a distinct advantage to BD compared to other simulation techniques. To trace the trajectories of about 100 ions interacting with a dielectric boundary for many microseconds, a period long enough to deduce the conductance of an ion channel, BD makes two simplifying assumptions. First, water is not treated explicitly but as a continuum. In reality, ions collide with neighboring water molecules incessantly and the net effects of these collisions are lumped together and treated as the frictional and random forces. Second, the atoms forming the channel are considered to be rigid whereas in reality they will undergo rapid thermal fluctuations. Several independent lines of evidence suggest that root-mean-square fluctuations of typical proteins are of the order of 0.75 Å, suggesting that the transmembrane passage through which ions traverse may be quite flexible (Allen et al., 2004; Noskov et al., 2004). By making these simplifications it is possible to measure channel conductances under various conditions and compare these measurements with experimental findings with only a modest amount of computational power.

Since the water and protein in BD are already represented as continuous media, the forces acting on charged particles are most often calculated by solving Poisson's

15. Brownian Dynamics

equation. A crucial issue is whether such a continuum approximation can be justified in a narrow, biological nanotube. In bulk water, molecules polarize so as to shield electrostatic interactions by a factor of approximately 1/80. However, given the likely preferential alignment of water in narrow pores and regions of high charge, this shielding is likely to be far less effective in an ion channel. Thus, one should use a lower value of the dielectric constant for the water in the channel when solving Poisson's equation. But exactly what value of the dielectric constant should be used is unknown. Determining the appropriate values using molecular dynamics simulations or otherwise would be a useful project.

Assigning the appropriate value of the dielectric constant of protein is also non-trivial. Unlike water and lipids, which form homogeneous media, proteins are quite heterogeneous, exhibiting large variations in polarizability depending on whether we are dealing with the interior or exterior of a protein (Schutz and Warshel, 2001). There are several molecular dynamics studies of the dielectric constant of protein (Smith et al., 1993; Simonson and Brooks, 1996; Pitera et al., 2001). The dielectric constant for the whole protein varies between 10 and 40, but when only the interior region of the protein consisting of the backbone and uncharged residues is considered, the value drops to 2 or 4. The effects of changing the dielectric constant of protein from 3.5 to 5 were examined by Chung et al. (2002a), using the KcsA potassium channel. They showed that the precise value adopted in solving Poisson's equation has negligible effects on the macroscopic properties derived from BD simulations.

The validity of treating the channel protein as a static structure in BD also deserves further investigation. It should be noted that thermal fluctuations of proteins occur in the time-scale of femtoseconds, whereas a conduction event across a typical ionic channel takes place once in 100 ns—approximately 6 to 7 orders of magnitude slower time-scale. Thus, it is likely that rapid thermal fluctuations of the atoms forming the channel are not important for channel selectivity and conduction. This can be formally proved using stochastic averaging methods in nonlinear dynamical systems (e.g., Sanders and Verhulst, 1985). Alterations in the average positions of the protein atoms caused by the presence of permeating ions may play a role, and their effects should be examined both experimentally and by using molecular dynamics simulations. If found to be important, some of the motions of the protein, such as the bending of carbonyl groups, can readily be incorporated in BD modeling of ion channels. Finally, size-dependent selectivity among ions with the same valence cannot be easily understood within the BD framework, and one has to appeal to molecular dynamics or semi-microscopic Monte Carlo simulations (Garofoli and Jordan, 2003; Jordan, 2005) for that purpose.

15.3 Application of Brownian Dynamics in Ion Channels

Despite the caveats to the use of BD, as outlined in the previous section, the technique has been fruitfully utilized in studying the dynamics of ion permeation in

Shin-Ho Chung and Vikram Krishnamurthy

a number of ion channels. An obvious application of BD is the calculation of current–voltage and conductance–concentration curves, which can be directly compared to the physiological measurements to assess the reliability and predictive power of the method. In addition to simple counting of ions crossing the channel, one can carry out a trajectory analysis of ions in the system to determine the steps involved in conduction. It is useful to find out the binding sites and the average number of ions in the channel, both of which are experimentally observable quantities. It is also possible to study the mechanisms of blocking of channels by larger molecules or other ion species. We summarize here some of the computational studies carried out on two important classes of biological ion channels—the KcsA potassium channel and ClC Cl[−] channel.

15.3.1 Potassium Channels

KcsA K⁺ Channel: To determine currents flowing across the channel, Chung et al. (1999, 2002a) and others (Mashl et al., 2001; Burykin et al., 2002) have performed BD simulations on the KcsA channel using the experimentally-determined channel structure. The shape of the ion-conducting pathway across the KcsA protein is illustrated in Fig. 15.1. The KcsA structure determined from X-ray diffraction consists of 396 amino acid residues, or 3504 atoms excluding polar hydrogens. The channel is constructed from four subunits of a tetramer of peptide chains, each subunit consisting of an outer helix, inner helix, pore helix, and a TVGYG (threonine–valine–glycine–tyrosine–glycine) amino acid sequence that forms the selectivity filter. The protein atoms form a central pore between these subunits. An outline of the pore reveals that the channel is composed of three segments—a long intracellular region of length 20 Å lined with hydrophobic amino acids extending toward the intracellular space (left-hand side in the Inset), a wide water-filled chamber of length 10 Å, and a narrow selectivity filter of length 12 Å, extending toward the extracellular space. The selectivity filter is the most important element in this structure as it can distinguish K⁺ ions from those of Na⁺ on the basis of their sizes (the crystal radius of K⁺ is 1.33 Å and that of Na⁺ is 0.95 Å). BD simulations show that there are three regions in the selectivity filter and cavity where K⁺ ions dwell preferentially (see Fig. 15.1). There is also another prominent binding site near the intracellular entrance of the channel. The preferred positions where ions dwell preferentially are in close agreement with the positions observed in Rb⁺ X-ray diffraction maps (Doyle et al., 1998).

To illustrate the permeation mechanism across the potassium channel, the channel is bisected such that ions in the chamber and filter are consigned to the right side, and the rest to the left side. The most common situation in the conducting state of the channel has one ion in the left half, and two ions in the right half. This configuration is referred to as the [1, 2] state. A typical conduction event consists of the following transitions: [1, 2]→[0, 3]→[0, 2]→[1, 2]. In other words, the ion waiting near the intracellular mouth overcomes a small energy barrier in the intracellular pore to enter the chamber region. Because this system is unstable in

15. Brownian Dynamics

the presence of an applied potential, the right-most ion is ejected from the channel. Another ion enters the intracellular mouth, leaving the system in its original configuration. The precise sequence of events taking place for conduction of ions depends on their concentration, applied potential and the ionization state of charged residues at the intracellular gate, and many other states can be involved in the conduction process depending on the values of these variables. Simulations also reveal that permeation across the filter is much faster than in other parts of the channel. That is, once a third ion reaches the oval cavity, the outermost ion in the selectivity filter is expelled almost instantaneously. Thus, although the filter plays a crucial role in selecting the K^+ ions, its role in influencing their conductance properties is minimal.

In Fig. 15.2A and B, we show the current–voltage and current–concentration curves obtained from BD simulations (Chung et al., 2002a). The results of BD simulations are in broad agreement with those determined experimentally (Coronado et al., 1980; Schrempf et al., 1995; Cuello et al., 1998; Heginbotham et al., 1999; Meuser et al., 1999; LeMasurier et al., 2001). When the radius of the intracellular gate of the crystal structure is expanded to 4 Å, the conductances at +150 mV and –150 mV are, respectively, 147 ± 7 and 96 ± 4 pS. The relationship is linear when the applied potential is in the physiological range but deviates from Ohm's law at a higher applied potential, especially at high positive potentials. The current saturates with increasing ionic concentrations, as shown in Fig. 15.2B. This arises because ion permeation across the channel is governed by two independent processes: the time it takes for an ion to enter the channel mouth depends on the concentration, while the time it takes for the ion to reach the oval chamber is independent of the concentration but depends solely on the applied potential.

Modeling other potassium channels: There are many different types of potassium channels, which differ widely in their conductances and gating characteristics while having a similar primary structure. Conductance levels of various types of potassium channels range from 4 to 270 pS (1 pS equals 0.1 pA of current across the channel with the driving force of 100 mV). Despite this diversity, they all share the common feature of being highly selective to potassium ions and display broadly similar selectivity sequences for monovalent cations.

To understand this feature, Chung et al. (2002b) investigated the possible structural differences that could give rise to different potassium channels. Using the experimentally determined potassium channel structure as a template, as shown in Fig. 15.3A, they systematically changed the radius of the intracellular pore entrance, leaving the dimensions of the selectivity filter and cavity unaltered. As the intrapore radius is increased from 2 to 5 Å, the channel conductance changes from 0.7 to 197 pS (0.17 to 48 pA). In Fig. 15.3B, the simulated current across the model ion channel determined from BD is plotted against the radius of the intrapore gate. By examining the energy profiles and the probabilities of ion occupancies in various segments of the channel, they deduce the rate-limiting step for conduction in the potassium channels. Ion distributions revealed that the selectivity filter is occupied by two K^+ ions most of the time. Potential energy profiles encountered by a third

Shin-Ho Chung and Vikram Krishnamurthy

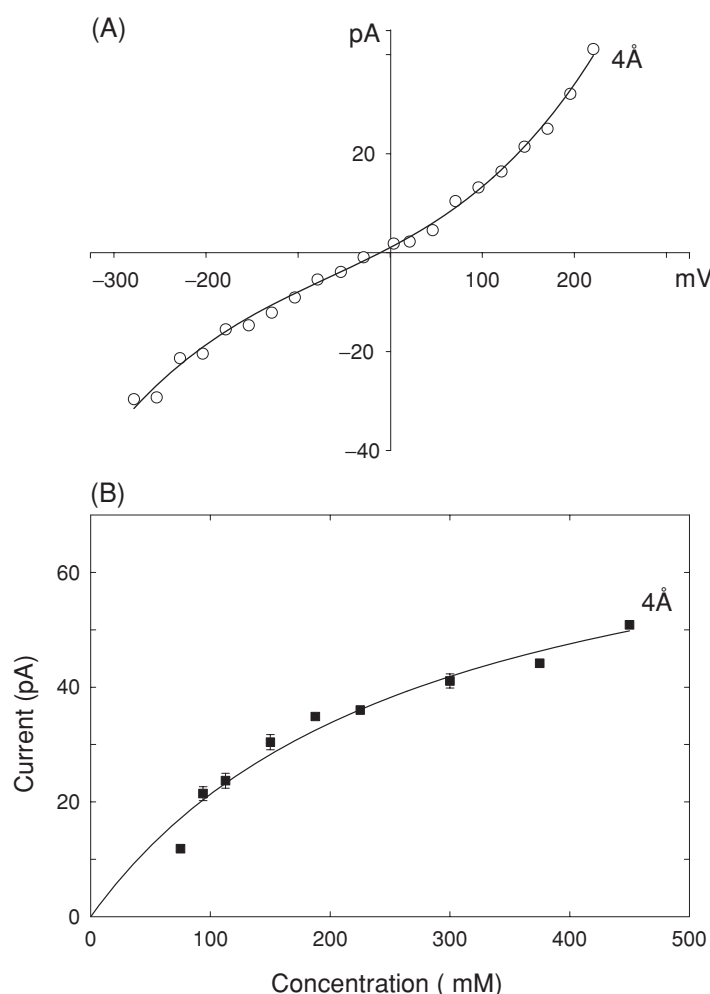


Fig. 15.2 The current–voltage–concentration profile of the K^+ channel with the intrapore radius of 4 Å. (A) The magnitude of current passing through the channel with symmetrical solution of 300 mM KCl in both reservoirs is plotted against the applied potential. (B) The outward currents are obtained with symmetrical solutions of varying concentrations of KCl in the reservoirs.

ion traversing along the central axis of the channel when there are two ions in or near the selectivity filter are shown for the channels with radii 2 Å (solid line in Fig. 15.3C), 3 Å (long-dashed line) and 4 Å (dashed line). Ions need to climb over the energy barrier, whose height is denoted as ΔU , to move across the channel. This barrier is the rate-limiting step in the permeation process: as its height increases with a decreasing intrapore radius, the channel conductance drops exponentially. Thus, the diversity of potassium channels seen in nature is achieved by slightly altering the geometry of the intracellular aspect of the channel macromolecule.

15. Brownian Dynamics

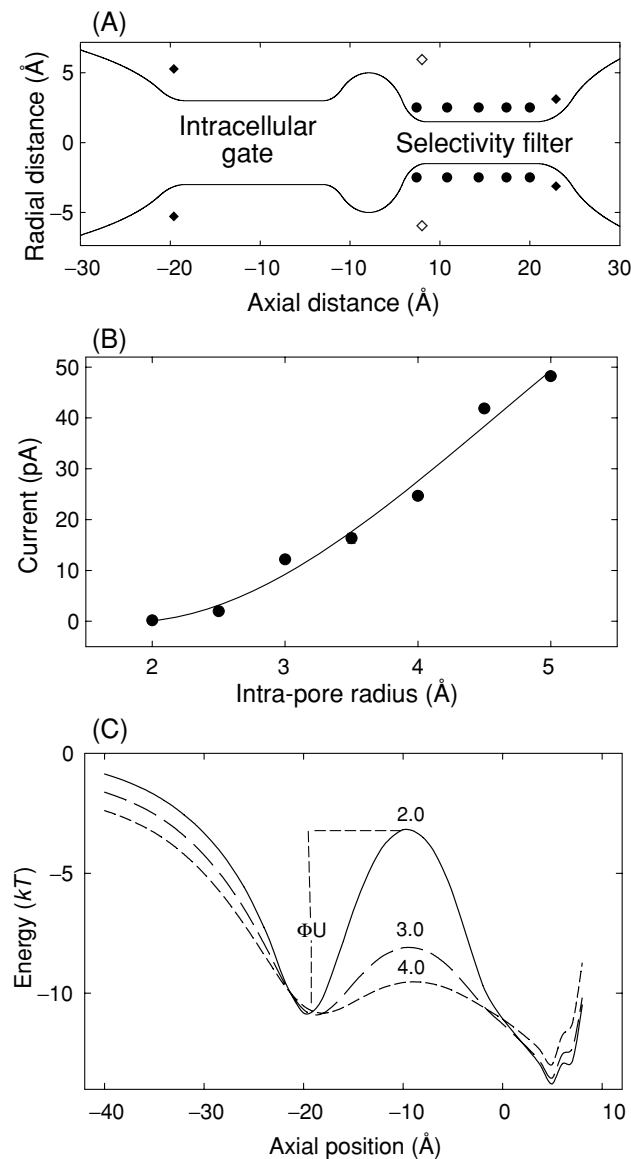


Fig. 15.3 Diversity of the potassium channels. (A) The shape of the KscA potassium is modified such that the minimal radius of the intracellular gate is 3 Å. The solid line shows the outline of a simplified model channel. The positions of dipoles on the channel wall are indicated. Filled circles are 10 of the 20 carbonyl oxygen atoms, open diamonds are N-termini of the helix dipole, and filled diamonds are mouth dipoles. (B) The dependence of outward channel currents on the intrapore radius of the channel is illustrated. The applied field to obtain the current is 2×10^7 V/m. (C) Potential energy profiles encountered by an ion traversing along the central axis of the channel when there are two other ions in or near the selectivity filter are shown for the channels with radii of 2 Å (solid line), 3 Å (long-dashed line) and 4 Å (dashed line). Ions need to climb over the energy barrier, whose height is denoted as ΔU , to move across the channel.

Shin-Ho Chung and Vikram Krishnamurthy

15.3.2 CIC Chloride Channels

BD simulations were similarly applied to elucidate the dynamics of ion permeation across CIC-type channels (Corry et al., 2004a,b). The prototype channel, known as CIC-0, first discovered and characterized by Miller (1982), is found in *Torpedo electroplax*. Since then, nine different human CIC genes and four plant and bacterial CIC genes have been identified. The CIC family of Cl^- channels is present in virtually all tissues—in muscle, heart, brain, kidney, and liver—and is widely expressed in most mammalian cells. By allowing Cl^- ions to cross the membrane, CIC channels perform diverse physiological roles, such as control of cellular excitability, cell volume regulation, and regulation of intracellular pH (Jenstsch et al., 1999; Maduke et al., 2000; Fahlke, 2001). Dutzler et al. (2002, 2003) determined the X-ray structure of a transmembrane CIC protein in bacteria, that has subsequently been shown to be a transporter, not an ion channel (Accardi and Miller, 2004). Nevertheless, many amino acid sequences of the bacterial CIC protein are conserved in their eukaryotic CIC relatives, which are selectively permeable to Cl^- ions.

Because the bacterial CIC protein shares many signature sequence identities with the eukaryotic CIC channels, it is possible to build homology models of these channels based on the structural information provided by Dutzler et al. (2002, 2003). With this aim in mind, Corry et al. (2004b) first altered the X-ray structure of the bacterial CIC protein using molecular dynamics to create an open-state configuration. They then converted to an open-state homology model of a eukaryotic CIC channel, CIC-0, using the crystal structure of the prokaryotic protein as a basis. As illustrated in Fig. 15.4A, the ionic pathway of CIC-0 takes a tortuous course through the protein, unlike that of the potassium channel, which is straight and perpendicular to the membrane surface. The channel is quite narrow, having a minimum radius of 2.5 Å near the center, but opens up quite rapidly at each end. The distance from one end of the pore to the other is 55 Å and it is lined with many charged and polar amino acid residues. Incorporating this homology model into BD, they determined the current–voltage–concentration profile of CIC-0. A current–voltage relationship obtained with symmetrical solutions of 150 mM in both reservoirs is shown in Fig. 15.4B. The relationship is linear, with a conductance of 11.3 ± 0.5 pS that agrees well with experimental measurements reported by Miller (1982) (superimposed open circles). The slope conductance determined from the experimental data is 9.4 ± 0.1 pS. The current–concentration relationship obtained from the homology model using BD (filled circles) is also accord with the experimental observations (obtained by Tsung-Yu Chen, personal communication) as shown in open circles in Fig. 15.4C. The lines fitted through the data points are calculated from the Michaelis–Menten equation. There is a reasonable agreement between the simulated data and experimental measurements for CIC-0.

BD simulations also reveal the steps involved in permeation of Cl^- ions across the CIC channel. The pore is normally occupied by two Cl^- ions. When a third ion enters the pore from the intracellular space (left-hand side in the Inset of Fig. 15.4A),

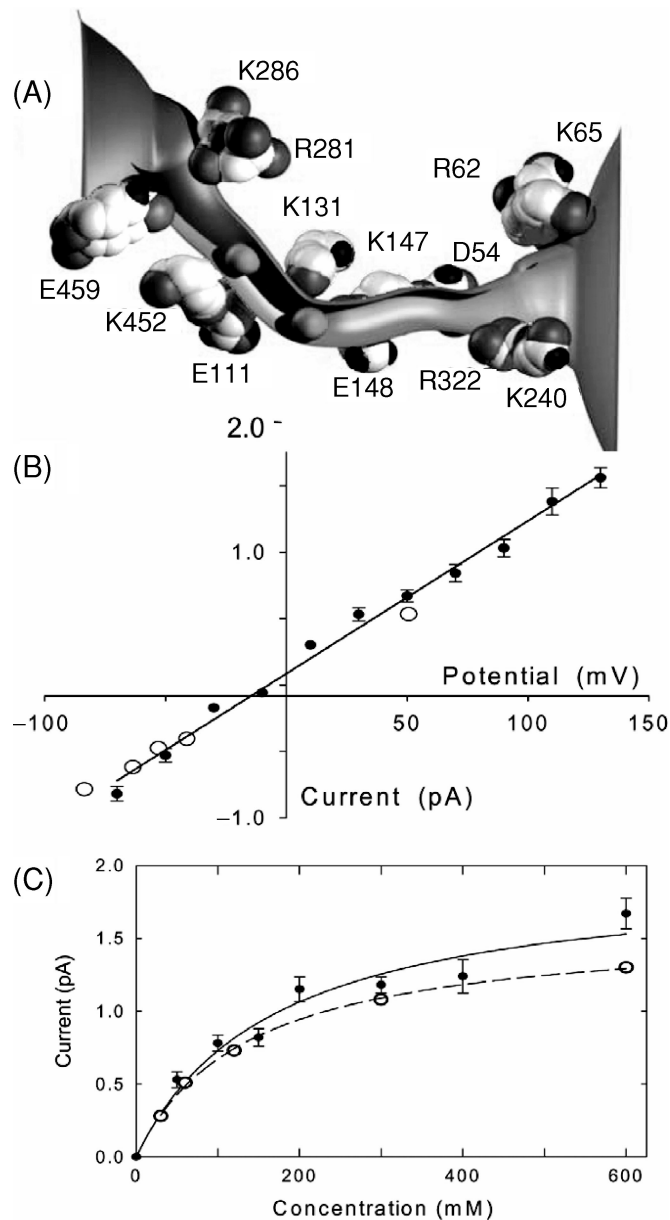


Fig. 15.4 Brownian dynamics simulations of an open-state ClC0 channel. (A) The water-filled pore of the channel through which Cl⁻ ions move is lined with both acidic and basic residues. The channel is normally occupied by two Cl⁻ ions, shown here in green. (B) The current-voltage relationship obtained from Brownian dynamics simulations (filled circles) is compared with the experimental data (open circles). (C) The current-concentration curve obtained with symmetrical solutions of varying concentrations of NaCl in the reservoirs under an applied potential of -80 mV (filled circles) is fitted with the Michaelis-Menten equation. The experimental measurements are shown in open circles. The half-saturation points determined from the fitted curves are 163 ± 51 mM for the simulated data and 136 ± 8 mM for the experimental data.

Shin-Ho Chung and Vikram Krishnamurthy

the stable equilibrium is disrupted, and the outermost Cl^- ion is expelled to the extracellular space.

15.4 Mathematical Formulation of Brownian Dynamics Algorithm

15.4.1 Overview

Here we provide a rigorous and mathematically complete formulation of the BD system for determining currents across a membrane ion channel. We prove that the continuous-time stochastic dynamical system, in which ions propagate via the Langevin equation, has a well-defined unique stationary distribution. We then show that the current across an ionic channel can be formulated in terms of mean passage rates of the ionic diffusion process, satisfying a boundary-valued partial differential equation, similar to the Fokker–Planck equation. We show that BD simulations can be viewed as a randomized algorithm for solving this partial differential equation to yield statistically consistent estimates of the currents flowing across an ionic channel.

Figure 15.5 shows the block diagram of BD simulation for permeation of ions through an ion channel. An iterative approach is used as follows: First, an initial estimate of the structural information of the channel, namely, the channel geometry and charges on the ionizable and polar residues in the protein are used to determine the parameters of Poisson's equation. Numerically solving Poisson's equation yields the potential of mean force (PMF) or energy landscape an ion traveling through the ion channel will experience. This in turn feeds into the BD simulation that

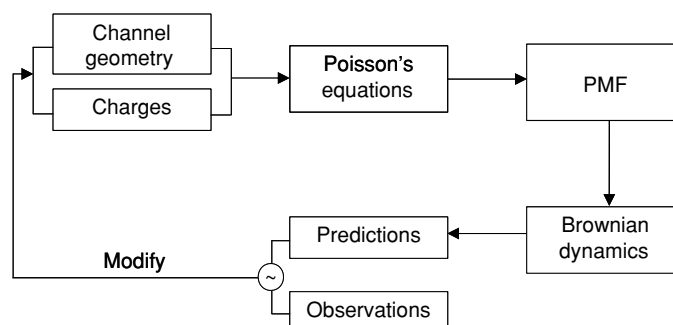


Fig. 15.5 A block diagram of the Brownian dynamics simulations. Using the channel shape of the channel and the charges on the atoms forming the protein, the profile of the potential of mean force along the central axis of the ion-conducting pathway is constructed by solving Poisson's equation. The currents derived from Brownian dynamics simulations are compared with those obtained experimentally. If there is a discrepancy between the simulated and experimental results, the channel geometry or the charges on atoms are modified and the procedure is repeated.

15. Brownian Dynamics

governs the stochastic evolution of all the ions. As a result of ions modeled by BD permeating through the ion channel, a simulated ion channel current is obtained. This simulated ion channel current is compared with the experimentally observed ion channel current. The difference between the two currents is used to refine our model of the channel geometry and charges and the process is repeated until the error between the simulated (predicted) ion channel current and experimentally determined ion channel current is minimized.

15.4.2 Mesoscopic Brownian Dynamics Formulation

The permeation model for the ion channel comprises two cylindrical reservoirs \mathcal{R}_1 and \mathcal{R}_2 connected by the ion channel \mathcal{C} as depicted in Fig. 15.6, in which $2N$ ions are inserted (N denotes a positive integer). As an example we have chosen the gramicidin pore, although the results below hold for any ion channel. Throughout, we index the $2N$ ions by $i = 1, 2, \dots, 2N$. These $2N$ ions comprise

- N positively charged ions indexed by $i = 1, 2, \dots, N$. Of these, $N/2$ ions indexed by $i = 1, 2, \dots, N/2$ are in \mathcal{R}_1 and $N/2$ ions indexed by $i = N/2 + 1, \dots, N$ are in \mathcal{R}_2 . Each Na^+ ion has charge q^+ , mass $m^{(i)} = m^+ = 3.8 \times 10^{-26}$ kg and frictional coefficient $m^+ \gamma^+$, and radius r^+ .
- N negatively charged ions. We index these by $i = N + 1, N + 2, \dots, 2N$. Of these, $N/2$ ions indexed by $i = N + 1, \dots, 3N/2$ are placed in \mathcal{R}_1 and the remaining $N/2$ ions indexed by $i = (3N/2) + 1, \dots, 2N$ are placed in \mathcal{R}_2 . Each negative ion has charge $q^{(i)} = q^-$, mass $m^{(i)} = m^-$, frictional coefficient $m^- \gamma^-$, and radius r^- .

Specifying the height of each reservoir to be $N \text{ \AA}$ guarantees that the concentration of ions in them is at the physiological concentration of 150 mM.

Let $t \geq 0$ denote continuous time. Each ion i moves in three-dimensional space over time. Let $\mathbf{x}_t^{(i)} = (x_t^{(i)}, y_t^{(i)}, z_t^{(i)})' \in \mathcal{R}$ and $\mathbf{v}_t^{(i)} \in \mathbb{R}^3$ denote the position and velocity of ion i at time t . Here and throughout this chapter all vectors are column vectors and denoted by the boldface font. Also we use $'$ to denote the transpose of a vector or matrix. The three components $x_t^{(i)}, y_t^{(i)}, z_t^{(i)}$ of $\mathbf{x}_t^{(i)} \in \mathbf{R}$ are, respectively, the x , y , and z position coordinates. Similarly, the three components of $\mathbf{v}_t^{(i)} \in \mathbb{R}^3$ are the x , y , z velocity components.

At time $t = 0$, the position $\mathbf{x}_0^{(i)}$ and velocity $\mathbf{v}_0^{(i)}$ of each of the $2N$ ions in the two reservoirs are randomly initialized as follows: The upper reservoir is divided into N cells of equal volume. In each cell is placed either one K^+ (or Na^+) or one Cl^- ion, each with probability half. The initial position $\mathbf{x}_0^{(i)}$ of ion i is chosen according to the uniform distribution within its cell. Similarly, the remaining $N/2$ K^+ ions $\{(N/2) + 1, \dots, N\}$ and remaining $N/2$ Cl^- ions $\{(3N/2) + 1, \dots, 2N\}$ are placed uniformly in the lower reservoir. This initialization of $\mathbf{x}_0^{(i)}$ emulates ensures that two particles are not placed too close to each other. The initial velocity vectors $\mathbf{v}_0^{(i)}$

Shin-Ho Chung and Vikram Krishnamurthy

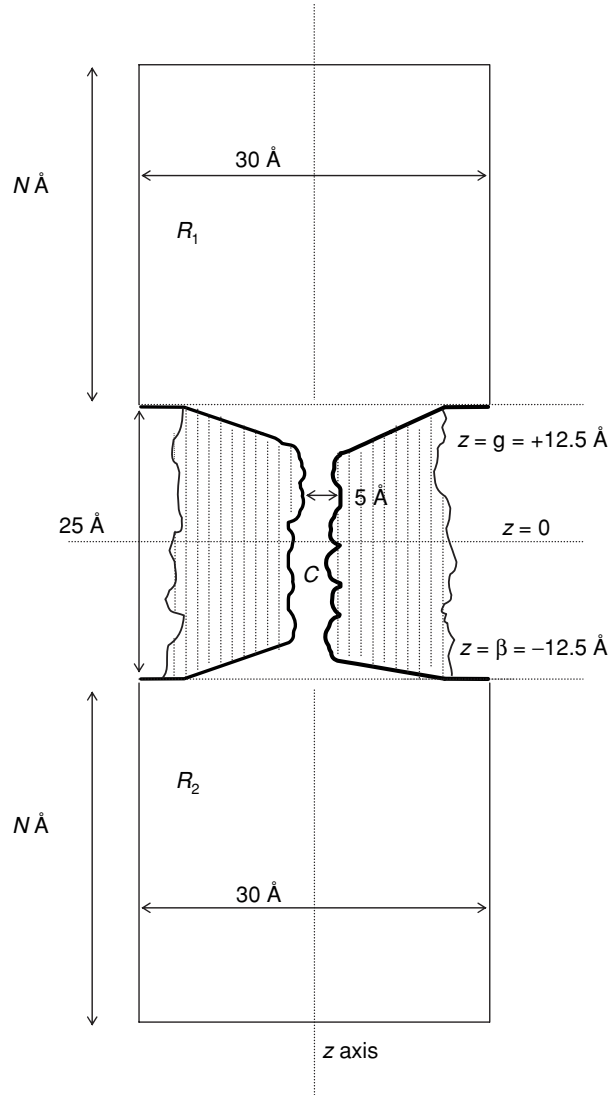


Fig. 15.6 A schematic illustration of a simulation assembly. The protein forming an ion channel, indicated with vertical dotted lines, is placed at the center of the assembly. For illustration, we use the gramicidin pore, whose length is approximately 25 Å. A reservoir, \mathcal{R}_1 and \mathcal{R}_2 , containing ions is attached at each end of the channel. The dimensions of each reservoir are indicated. The two reservoirs are connected via a conduit formed by the channel protein \mathcal{C} .

of the $2N$ ions are typically initialized according to a three-dimensional Gaussian distribution with zero mean, and 3×3 diagonal positive definite covariance matrix. Thus the distribution of the magnitude of the initial velocity $|\mathbf{v}_0^{(i)}|$ has a Maxwell density.

15. Brownian Dynamics

An external potential $\Phi(\mathbf{x})$ is applied along the z axis of Fig. 15.6, i.e., with $\mathbf{x} = (x, y, z)$,

$$\Phi_{\lambda}^{\text{ext}}(\mathbf{x}) = -E^{\text{ext}}z \quad (15.1)$$

where $-E^{\text{ext}}$ is the external field in V/m in z direction. Applied potential λ is related to E^{ext} by $E^{\text{ext}} = -\lambda/l$, where l is the length of the channel, and $\lambda \in \Lambda$. Here, Λ denotes a finite set of applied potentials. Typically, $\Lambda = \{-200, -180, \dots, 0, \dots, 180, 200\}$ mV/m. Due to this applied external potential, K^+ ions drift from reservoir \mathcal{R}_1 to \mathcal{R}_2 via the ion channel \mathcal{C} in Fig. 15.6.

Let $\mathbf{X}_t = (\mathbf{x}_t^{(1)'}, \mathbf{x}_t^{(2)'}, \mathbf{x}_t^{(3)'}, \dots, \mathbf{x}_t^{(2N)'})' \in \mathcal{R}^{2N}$ denote the positions and $\mathbf{V}_t = (\mathbf{v}_t^{(1)'}, \mathbf{v}_t^{(2)'}, \mathbf{v}_t^{(3)'}, \dots, \mathbf{v}_t^{(2N)'})' \in \mathbb{R}^{6N}$ denote the velocities of all the $2N$ ions at time $t \geq 0$. The position and velocity of each individual ion evolves according to the following continuous time stochastic dynamical system (recall $i = 1, 2, \dots, N$ denote positive ions and $i = N + 1, \dots, 2N$ denote negative ions):

$$\mathbf{x}_t^{(i)} = \mathbf{x}_0^{(i)} + \int_0^t \mathbf{v}_s^{(i)} ds, \quad (15.2)$$

$$m^+ \mathbf{v}_t^{(i)} = m^+ \mathbf{v}_0^{(i)} - \int_0^t m^+ \gamma^+(\mathbf{x}_s^{(i)}) \mathbf{v}_s^{(i)} ds + \int_0^t F_{\theta, \lambda}^{(i)}(\mathbf{X}_s) ds + b^+(\mathbf{x}_s^{(i)}) \mathbf{w}_s^{(i)}, \quad (15.3)$$

$$m^- \mathbf{v}_t^{(i)} = m^- \mathbf{v}_0^{(i)} - \int_0^t m^- \gamma^-(\mathbf{x}_s^{(i)}) \mathbf{v}_s^{(i)} ds + \int_0^t F_{\theta, \lambda}^{(i)}(\mathbf{X}_s) ds + b^-(\mathbf{x}_s^{(i)}) \mathbf{w}_s^{(i)}, \quad (15.4)$$

where $\gamma^{\pm}(\mathbf{x}_s^{(i)}) = \gamma^{\pm}$ (defined in the beginning of this section) if the ion is in the reservoir, and $\gamma(\mathbf{x}_s^{(i)})$ is determined by molecular dynamics simulation when the ion is in the ion channel (Allen et al., 2000). Eq. 15.2 says that velocity is the time derivative of the position. Eqs. 15.3 and 15.4 constitute the well-known *Langevin* equations. We now describe the various quantities in the above equations.

In Eqs. 15.3 and 15.4, the process $\{\mathbf{w}_t^{(i)}\}$ denotes a three-dimensional zero mean Brownian motion, which is component-wise independent. The constants b^+ and b^- are, respectively,

$$b^{+2}(\mathbf{x}_s^{(i)}) = 2m^+ \gamma^+(\mathbf{x}_s^{(i)}) kT, \quad b^{-2}(\mathbf{x}_s^{(i)}) = 2m^- \gamma^-(\mathbf{x}_s^{(i)}) kT. \quad (15.5)$$

The noise processes $\{\mathbf{w}_t^{(i)}\}$ and $\{\mathbf{w}_t^{(j)}\}$, that drive any two different ions, $j \neq i$, are assumed to be statistically independent.

In Eqs. 15.3 and 15.4, $F_{\theta, \lambda}^{(i)}(\mathbf{X}_t) = -q^{(i)} \nabla_{\mathbf{x}_t^{(i)}} \Phi_{\theta, \lambda}^{(i)}(\mathbf{X}_t)$ represents the *systematic force* acting on ion i , where the scalar-valued process $\Phi_{\theta, \lambda}^{(i)}(\mathbf{X}_t)$ is the total electric potential experienced by ion i given the position \mathbf{X}_t of the $2N$ ions. The subscript λ is the applied external potential in Eq. 15.1. The subscript θ is a parameter vector that characterizes the PMF, which is an important component of $\Phi_{\theta, \lambda}^{(i)}(\mathbf{X}_t)$. As described

Shin-Ho Chung and Vikram Krishnamurthy

below, $F_{\theta,\lambda}^{(i)}(\mathbf{X}_t)$ includes an ion-wall interaction force that ensures that position $\mathbf{x}_t^{(i)}$ of each ion lies in \mathcal{R} —see Eq. 15.9 below.

It is notationally convenient to represent the above system, Eqs. 15.2, 15.3 and 15.4 as a vector stochastic differential equation. Define the following vector-valued variables:

$$\mathbf{V}_t = \begin{bmatrix} \mathbf{V}_t^+ \\ \mathbf{V}_t^- \end{bmatrix}, \text{ where } \mathbf{V}_t^+ = \begin{bmatrix} \mathbf{v}_t^{(1)} \\ \vdots \\ \mathbf{v}_t^{(N)} \end{bmatrix}, \mathbf{V}_t^- = \begin{bmatrix} \mathbf{v}_t^{(N+1)} \\ \vdots \\ \mathbf{v}_t^{(2N)} \end{bmatrix}, \mathbf{w}_t = \begin{bmatrix} \mathbf{0}_{2N \times 1} \\ \mathbf{w}_t^{(1)} \\ \vdots \\ \mathbf{w}_t^{(2N)} \end{bmatrix},$$

$$\boldsymbol{\zeta}_t = \begin{bmatrix} \mathbf{X}_t \\ \mathbf{V}_t^+ \\ \mathbf{V}_t^- \end{bmatrix}, \mathbf{F}_{\theta,\lambda}^+(\mathbf{X}_t) = \begin{bmatrix} F_{\theta,\lambda}^{(1)}(\mathbf{X}_t) \\ \vdots \\ F_{\theta,\lambda}^{(N)}(\mathbf{X}_t) \end{bmatrix}, \mathbf{F}_{\theta,\lambda}^-(\mathbf{X}_t) = \begin{bmatrix} F_{\theta,\lambda}^{(N+1)}(\mathbf{X}_t) \\ \vdots \\ F_{\theta,\lambda}^{(2N)}(\mathbf{X}_t) \end{bmatrix}. \quad (15.6)$$

The above system, namely, Eqs. 15.2, 15.3, 15.4 can be written as

$$\boldsymbol{\zeta}_t = \boldsymbol{\zeta}_0 + \int_0^t \mathbf{A}(\mathbf{X}_\tau) \boldsymbol{\zeta}_\tau d\tau + \int_0^t \mathbf{f}(\boldsymbol{\zeta}_\tau) d\tau + \Sigma^{1/2}(\mathbf{X}_\tau) \mathbf{w}_\tau \quad (15.7)$$

where $\Sigma^{1/2}(\mathbf{X}_\tau) = \text{diag}(\mathbf{0}_{6N \times 6N}, b^+(\mathbf{X}_\tau)/m^+, b^-(\mathbf{X}_\tau)/m^-)$, I_{6N} denotes the $6N \times 6N$ identity matrix,

$$\mathbf{A} = \begin{bmatrix} \mathbf{0}_{6N \times 6N} & \mathbf{I}_{6N} \\ \mathbf{0}_{6N \times 6N} & \begin{bmatrix} -\gamma^+(\mathbf{X}_\tau) & \mathbf{0}_{3N \times 3N} \\ \mathbf{0}_{3N \times 3N} & -\gamma^-(\mathbf{X}_\tau) \end{bmatrix} \end{bmatrix}, \quad \mathbf{f}(\boldsymbol{\zeta}_t) = \begin{bmatrix} \mathbf{0}_{6N \times 1} \\ \frac{1}{m^+} \mathbf{F}_{\theta,\lambda}^+(\mathbf{X}_t) \\ \frac{1}{m^-} \mathbf{F}_{\theta,\lambda}^-(\mathbf{X}_t) \end{bmatrix}. \quad (15.8)$$

We will subsequently refer to Eqs. 15.7 and 15.8 as the BD equations for a biological ion channel.

Remark: Another way of ensuring that the positions $\mathbf{x}_t^{(i)}$ of all ions are in \mathcal{R}^o is to introduce a reflection term \mathbf{Z}_t that models elastic collisions at the boundary of \mathcal{R} . However, as described below, the ion wall systematic interaction force ensures that all ions remain in \mathcal{R}^o . Hence we do not consider a reflected diffusion formulation in this chapters.

15.4.3 Systematic Force Acting on Ions

As mentioned after Eq. 15.4, the systematic force experienced by each ion i is

$$\mathbf{F}_{\theta,\lambda}^{(i)}(\mathbf{X}_t) = -q^{(i)} \nabla_{\mathbf{x}_t^{(i)}} \Phi_{\theta,\lambda}^{(i)}(\mathbf{X}_t),$$

15. Brownian Dynamics

where the scalar-valued process $\Phi_{\theta,\lambda}^{(i)}(\mathbf{X}_t)$ denotes the total electric potential experienced by ion i given the position \mathbf{X}_t of all the $2N$ ions. We now give a detailed formulation of these systematic forces.

The potential $\Phi_{\theta,\lambda}^{(i)}(\mathbf{X}_t)$ experienced by each ion i comprises the following five components:

$$\Phi_{\theta,\lambda}^{(i)}(\mathbf{X}_t) = U_\theta(\mathbf{x}_t^{(i)}) + \Phi_\lambda^{\text{ext}}(\mathbf{x}_t^{(i)}) + \Phi^{IW}(\mathbf{x}_t^{(i)}) + \Phi^{C,i}(\mathbf{X}_t) + \Phi^{SR,i}(\mathbf{X}_t). \quad (15.9)$$

Just as $\Phi_{\theta,\lambda}^{(i)}(\mathbf{X}_t)$ is decomposed into five terms, we can similarly decompose the force $F_{\theta,\lambda}^{(i)}(\mathbf{X}_t) = -q \nabla_{\mathbf{x}_t^{(i)}} \Phi_{\theta,\lambda}^{(i)}(\mathbf{X}_t)$ experienced by ion i as the superposition (vector sum) of five force terms, where each force term is due to the corresponding potential in Eq. 15.9—however, for notational simplicity we describe the scalar-valued potentials rather than the vector-valued forces.

Note that the first three terms in Eq. 15.9, namely $U_\theta(\mathbf{x}_t^{(i)})$, $\Phi_\lambda^{\text{ext}}(\mathbf{x}_t^{(i)})$, $\Phi^{IW}(\mathbf{x}_t^{(i)})$ depend only on the position $\mathbf{x}_t^{(i)}$ of ion i , whereas the last two terms in Eq. 15.9 $\Phi^{C,i}(\mathbf{X}_t)$, $\Phi^{SR,i}(\mathbf{X}_t)$ depend on the distance of ion i to all the other ions, namely, the position \mathbf{X}_t of all the ions. The five components in Eq. 15.9 are now defined.

- (i) *Potential of mean force (PMF)*, denoted $U_\theta(\mathbf{x}_t^{(i)})$ in Eq. 15.9, comprises electric forces acting on ion i when it is in or near the ion channel (nanotube) \mathcal{C} in Fig. 15.6. The PMF U_θ is a smooth function of the ion position $\mathbf{x}_t^{(i)}$ and depends on the structure of the ion channel. Therefore, estimating $U_\theta(\cdot)$ yields structural information about the ion channel. The PMF U_θ originates from fixed charges in the channel protein and surface charges induced by mobile ions.
- (ii) *External applied potential*: In the vicinity of living cells, there is a strong electric field resulting from the membrane potential, which is generated by diffuse, unpaired, ionic clouds on each side of the membrane. Typically, this resting potential across a cell membrane, whose thickness is about 50 \AA , is 70 mV , the cell interior being negative with respect to the extracellular space.

For ion i at position $\mathbf{x}_t^{(i)} = (x, y, z)$, $\Phi_\lambda^{\text{ext}}(\mathbf{x}) = \lambda z$ (see Eq. 15.1) denotes the potential on ion i due to the applied external field. The electrical field acting on each ion due to the applied potential is therefore $-\nabla_{\mathbf{x}_t^{(i)}} \Phi_\lambda^{\text{ext}} = (0, 0, \lambda) \text{ V/m}$ at all $\mathbf{x} \in \mathcal{R}$. It is this applied external field that causes a drift of ions from the reservoir \mathcal{R}_1 to \mathcal{R}_2 via the ion channel \mathcal{C} . As a result of this drift of ions within the electrolyte in the two reservoirs, eventually the measured potential drop across the reservoirs is zero and all the potential drop occurs across the ion channel.

- (iii) *Inter-ion Coulomb potential*: In Eq. 15.9, $\Phi^{C,i}(\mathbf{X}_t)$ denotes the Coulomb interaction between ion i and all the other ions.

$$\Phi^{C,i}(\mathbf{X}_t) = \frac{1}{4\pi\epsilon_0} \sum_{j=1, j \neq i}^{2N} \frac{q^{(j)}}{\epsilon_w \|\mathbf{x}_t^{(i)} - \mathbf{x}_t^{(j)}\|} \quad (15.10)$$

Shin-Ho Chung and Vikram Krishnamurthy

- (iv) *Ion-wall interaction potential*: The ion-wall potential Φ^{IW} , also called the $(\sigma/r)^9$ potential, ensures that the position of all ions $i = 1, \dots, 2N$ lie in \mathcal{R}^o . With $\mathbf{x}_t^{(i)} = (x_t^{(i)}, y_t^{(i)}, z_t^{(i)})'$, it is modeled as

$$\Phi^{IW}(\mathbf{x}_t^{(i)}) = \frac{F_0}{9} \frac{(r^{(i)} + r_w)^9}{\left[r_c + r_w - \left(\sqrt{(x_t^{(i)})^2 + (y_t^{(i)})^2} \right) \right]^9}, \quad (15.11)$$

where for positive ions $r^{(i)} = r^+$ (radius of K^+ atom) and for negative ions $r^{(i)} = r^-$ (radius of Cl^- atom), $r_w = 1.4 \text{ \AA}$ is the radius of atoms making up the wall, r_c denotes the radius of the ion channel, and $F_0 = 2 \times 10^{-10} \text{ N}$ which is estimated from the ST2 water model used in molecular dynamics (Stillinger and Rahman, 1974). This ion-wall potential results in short-range forces that are only significant when the ion is close to the wall of the reservoirs \mathcal{R}_1 and \mathcal{R}_2 or anywhere in the ion channel \mathcal{C} (since the narrow segment of an ion channel can be comparable in radius to the ions).

- (v) *Short-range potential*: Finally, at short ranges, the Coulomb interaction between two ions is modified by adding a potential $\Phi^{SR,i}(\mathbf{X}_t)$, which replicates the effects of the overlap of electron clouds. Thus,

$$\Phi^{SR,i}(\mathbf{X}_t) = \frac{F_0}{9} \sum_{j=1, j \neq i}^{2N} \frac{(r^{(i)} + r^{(j)})}{\|\mathbf{x}_t^{(i)} - \mathbf{x}_t^{(j)}\|^9}. \quad (15.12)$$

Similar to the ion-wall potential, $\Phi^{SR,i}$ is significant only when ion i gets very close to another ion. It ensures that two opposite charge ions attracted by inter-ion Coulomb forces (Eq. 15.10) cannot collide and annihilate each other. Molecular dynamics simulations show that the hydration forces between two ions add further structure to the $1/\|\mathbf{x}_t^{(i)} - \mathbf{x}_t^{(j)}\|^9$ repulsive potential due to the overlap of electron clouds in the form of damped oscillations (Guàrdia et al., 1991a, b). Corry et al. (2001) incorporated the effect of the hydration forces in Eq. 15.12 in such a way that the maxima of the radial distribution functions for $\text{Na}^+ - \text{Na}^+$, $\text{Na}^+ - \text{Cl}^-$, and $\text{Cl}^- - \text{Cl}^-$ would correspond to the values obtained experimentally.

15.5 Probabilistic Characterization of Channel Conductance

Thus far, Eqs. 15.7–15.9 give a complete description of the stochastic dynamics of the ions. We now demonstrate here that the mean ion channel current satisfies a boundary-valued partial differential equation related to the Fokker–Planck equation. There are two main results in this section that logically progress toward deriving this

15. Brownian Dynamics

partial differential equation. Theorem 1 shows that the BD system, given in Eq. 15.7, converges exponentially fast to a unique stationary distribution. Theorem 3 gives a characterization for the ion channel current in terms of the mean first passage time of the diffusion process (Eq. 15.7).

To motivate these results, we first formalize mathematically the construction of the BD simulation. There are two key requirements that a mathematical construction of the BD simulation should take into account: First, the concentration of ions in each reservoir \mathcal{R}_1 and \mathcal{R}_2 should remain approximately constant and equal to the physiological concentration. Note that if the system was allowed to evolve for an infinite time with the channel open, then eventually due to the external applied potential, more ions will be in \mathcal{R}_2 than \mathcal{R}_1 . This would violate the condition that the concentration of particles in \mathcal{R}_1 and \mathcal{R}_2 remain constant.

Second, the dynamics of the BD simulation has an inherent two-time scale property. Typically, the time for an ion to enter and propagate through the ion channel is at least an order of magnitude larger compared to the time it takes for an ion to move within a reservoir. That is, the time constant for the particles in the reservoirs to attain steady state is much smaller than the time it takes for a particle to enter and propagate through the channel.

The following two step probabilistic construction formalizes the above two requirements and ensures that they are satisfied.

Procedure 1: Probabilistic construction of Brownian dynamics ion permeation in ion channels

- *Step 1:* The $2N$ ions in the system are initialized as described in Eq. 15.1 and the ion channel \mathcal{C} is closed. The system evolves and attains stationarity. Theorem 1 below shows that the probability density function of the $2N$ particles converges exponentially fast to a unique stationary distribution. Theorem 3 shows that in the stationary regime, all positive ions in reservoir \mathcal{R}_1 have the same stationary distribution and so are statistically indistinguishable (similarly for \mathcal{R}_2).
- *Step 2:* After stationarity is achieved, the ion channel is opened. The ions evolve according to Eq. 15.7. As soon as an ion from \mathcal{R}_1 crosses the ion channel \mathcal{C} and enters \mathcal{R}_2 , the experiment is stopped. Similarly, if an ion from \mathcal{R}_2 crosses \mathcal{C} and enters \mathcal{R}_1 , the experiment is stopped. Theorem 3 gives partial differential equations for the mean time an ion in \mathcal{R}_1 takes to cross the ion channel and reach \mathcal{R}_2 (and for the time it takes an ion to cross from \mathcal{R}_2 to \mathcal{R}_1). From this a theoretical expression for the mean ion channel current is constructed (Eq. 15.24).

These two steps constitute one iteration of the BD simulation Algorithm 1. The construction of restarting the simulation each time an ion crosses the channel ensures that the random amount of time for an ion to cross the ion channel in any BD simulation iteration is statistically independent of the time for any other iteration. This statistical independence will be exploited in Theorem 3 to show that the BD algorithm yields statistically consistent estimates of the ion channel current.

Shin-Ho Chung and Vikram Krishnamurthy

Remarks. The above construction is a mathematical idealization. In actual BD algorithms, the ion channel is kept open and ions that cross the channel are simply removed and replaced in their original reservoir. However, as described later (following Algorithm 1), the above mathematical construction is an excellent approximation due to the fact that by virtue of Step 1, the system of particles with the newly replaced ion converges exponentially fast to its stationary distribution, and by virtue of the two time scale property, the time taken to attain this stationary distribution is much less than the time it takes for a single ion to cross the ion channel.

With the above mathematical construction of the BD simulation, we now proceed to stating and proving the main results. Let

$$\pi_t^{(\theta, \lambda)}(\mathbf{X}, (\mathbf{V})) = p^{(\theta, \lambda)}(\mathbf{x}_t^{(1)}, \mathbf{x}_t^{(2)}, \dots, \mathbf{x}_t^{(2N)}, \mathbf{v}_t^{(1)}, \mathbf{v}_t^{(2)}, \dots, \mathbf{v}_t^{(2N)}) \quad (15.13)$$

denote the joint probability density function of the position and velocity of all the $2N$ ions at time t . We explicitly denote the θ, λ dependence of the probability density functions since they depend on the PMF U_θ and applied external potential λ . Note that the marginal probability density function $\pi_t^{(\theta, \lambda)}(\mathbf{X}) = p_t^{(\theta, \lambda)}(\mathbf{x}_t^{(1)}, \mathbf{x}_t^{(2)}, \dots, \mathbf{x}_t^{(2N)})$ of the positions of all $2N$ ions at time t is obtained as

$$\pi_t^{(\theta, \lambda)}(\mathbf{X}) = \int_{\mathbb{R}^{6N}} \pi_t^{(\theta, \lambda)}(\mathbf{X}, (\mathbf{V})) d\mathbf{V}.$$

The following result, the proof of which is not given here, states that for the above stochastic dynamical system, $\pi_t^{(\theta, \lambda)}(\mathbf{X}, \mathbf{V})d\mathbf{V}$ converges exponentially fast to its stationary (invariant) distribution $\pi_\infty^{(\theta, \lambda)}(\mathbf{X}, V)$. That is, the ions in the two reservoirs attain steady state exponentially fast.

Theorem 1. *Consider Step 1 of the BD probabilistic construction in Procedure 1. For the BD system, represented in Eqs. 15.7 and 15.8, comprising $2N$ ions, with $\zeta = (\mathbf{X}, \mathbf{V})$, there exists a unique stationary distribution $\pi_\infty^{(\theta, \lambda)}(\zeta)$, and constants $K > 0$ and $0 < \rho < 1$, such that*

$$\sup_{\zeta \in \mathcal{R}^{2N} \times \mathbb{R}^{6N}} |\pi_t^{(\theta, \lambda)}(\zeta) - \pi_\infty^{(\theta, \lambda)}(\zeta)| \leq K \mathcal{V}(\zeta) \rho^t. \quad (15.14)$$

Here $\mathcal{V}(\zeta) > 1$ is an arbitrary measurable function on $\mathcal{R}^{2N} \times \mathbb{R}^{6N}$.

The next result to establish is, under the conditions of Step 1, the ions in the two reservoirs are statistically indistinguishable. Let us first introduce the following notation and the Fokker–Planck equation.

Notation. For $\zeta = (\zeta^{(1)}, \dots, \zeta^{(4N)})'$, define the gradient operator

$$\nabla_\zeta = \left(\frac{\partial}{\partial \zeta^{(1)}}, \frac{\partial}{\partial \zeta^{(2)}}, \dots, \frac{\partial}{\partial \zeta^{(4N)}} \right)'$$

15. Brownian Dynamics

For a vector field $\mathbf{f}(\zeta) = [f^{(1)}(\zeta) \ f^{(2)}(\zeta) \ \cdots \ f^{(4N)}(\zeta)]'$ defined on \mathbb{R}^{4N} , define the divergence operator

$$\operatorname{div}(\mathbf{f}_{\theta,\lambda}) = \frac{\partial f^{(1)}}{\partial \zeta^{(1)}} + \frac{\partial f^{(2)}}{\partial \zeta^{(2)}} + \cdots + \frac{\partial f^{(4N)}}{\partial \zeta^{(4N)}}. \quad (15.15)$$

For the stochastic dynamical system (Eq. 15.7) comprising of $2N$ ions, define the backward elliptic operator (infinitesimal generator) \mathcal{L} and its adjoint \mathcal{L}^* for any test function $\phi(\zeta)$ as

$$\begin{aligned} \mathcal{L}(\phi) &= \frac{1}{2} \operatorname{Tr}[\Sigma \nabla_{\zeta}^2 \phi(\zeta)] + (\mathbf{f}_{\theta,\lambda}(\zeta) + \mathbf{A}\zeta)' \nabla_{\zeta} \phi(\zeta) \\ \mathcal{L}^*(\phi) &= \frac{1}{2} \operatorname{Tr}[\nabla_{\zeta}^2 (\Sigma \phi(\zeta))] - \operatorname{div}[(\mathbf{A}\zeta + \mathbf{f}_{\theta,\lambda}(\zeta))\phi(\zeta)]. \end{aligned} \quad (15.16)$$

Here, $\mathbf{f}_{\theta,\lambda}$ and Σ are defined in Eq. 15.8. We refer the reader to Karatzas and Shreve (1991) for an exposition of stochastic differential equations driven by Brownian motion.

It is well known that the probability density function $\pi_t^{(\theta,\lambda)}(\cdot)$ of the $2N$ ions where $\zeta_t = (\mathbf{X}_t', \mathbf{V}_t')'$ (defined in Eq. 15.13) satisfies the Fokker–Planck equation (Wong and Hajek, 1985):

$$\frac{\partial \pi_t^{(\theta,\lambda)}}{\partial t} = \mathcal{L}^* \pi_t^{(\theta,\lambda)}, \quad (15.17)$$

where $\pi_0^{(\theta,\lambda)}$ is initialized as described in Eq. 15.1. We refer the reader to Wong and Hajek (1985) for an excellent treatment of the Fokker–Planck equation. Briefly, the Fokker–Planck equation may be merely viewed as a partial differential equation (involving derivatives with respect to the state ζ and time t) that determines the time evolution of the probability density function $\pi_t^{(\theta,\lambda)}$.

Also, the stationary probability density function $\pi_{\infty}^{(\theta,\lambda)}(\cdot)$ satisfies

$$\mathcal{L}^*(\pi_{\infty}^{(\theta,\lambda)}) = 0, \quad \int_{\mathbb{R}^{6N}} \int_{\mathcal{R}^{2N}} \pi_{\infty}^{(\theta,\lambda)}(\mathbf{X}, \mathbf{V}) d\mathbf{X} d\mathbf{V} = 1 \quad (15.18)$$

The intuition behind this is that if $\pi_t^{(\theta,\lambda)}$ attains “steady state” (stationarity), it no longer evolves with time, i.e., its derivative with respect to time is zero. Hence, setting the left-hand side of Eq. (15.17) to zero yields the above equation.

We next show that once stationarity has been achieved in Step 1, the N positive ions behave statistically identically, i.e., each ion has the same stationary marginal

Shin-Ho Chung and Vikram Krishnamurthy

distribution. Define the stationary marginal density $\pi_{\infty}^{(\theta, \lambda)}(\mathbf{x}^{(i)}, \mathbf{v}^{(i)})$ of ion i as

$$\pi_{\infty}^{(\theta, \lambda)}(\mathbf{x}^{(i)}, \mathbf{v}^{(i)}) = \int_{\mathbb{R}^{6N-3}} \int_{\mathcal{R}^{2N-1}} \pi_{\infty}^{(\theta, \lambda)}(\mathbf{X}, \mathbf{V}) \prod_{j=1, j \neq i}^{2n} d\mathbf{x}^{(j)} d\mathbf{v}^{(j)} \quad (15.19)$$

We state the following result without the proof.

Theorem 2. *Consider Step 1 of the BD probabilistic construction in Procedure 1. Then the stationary marginal densities for the positive ions in \mathcal{R}_1 are identical:*

$$\pi_{\infty}^{(\theta, \lambda), \mathcal{R}_1} \equiv \pi_{\infty}^{(\theta, \lambda)}(\mathbf{x}^{(1)}, \mathbf{v}^{(1)}) = \pi_{\infty}^{(\theta, \lambda)}(\mathbf{x}^{(2)}, \mathbf{v}^{(2)}) = \dots = \pi_{\infty}^{(\theta, \lambda)}(\mathbf{x}^{(N)}, \mathbf{v}^{(N/2)}). \quad (15.20)$$

Similarly, the stationary marginal densities for the positive ions in \mathcal{R}_2 are identical:

$$\begin{aligned} \pi_{\infty}^{(\theta, \lambda), \mathcal{R}_2} &\equiv \pi_{\infty}^{(\theta, \lambda)}(\mathbf{x}^{(N/2+1)}, \mathbf{v}^{(N/2+1)}) = \pi_{\infty}^{(\theta, \lambda)}(\mathbf{x}^{(N/2+2)}, \mathbf{v}^{(N/2+2)}) \\ &= \dots = \pi_{\infty}^{(\theta, \lambda)}(\mathbf{x}^{(N)}, \mathbf{v}^{(N)}). \end{aligned} \quad (15.21)$$

Theorem 2 is not surprising—as Eqs. 15.2, 15.3 and 15.4 are symmetric in i , one would intuitively expect that once steady state has been attained, all the positive ions behave identically—similarly with the negative ions. Due to above result, once the system has attained steady state, any positive ion is representative of all the N positive ions, and similarly for the negative ions.

Having discussed Step 1, we now proceed to Step 2 of the BD probabilistic construction of Procedure 1. Assume that the system (Eq. 15.7) comprising $2N$ ions has attained stationarity with the ion channel \mathcal{C} closed according to Step 1. Now in Step 2 of Procedure 1, the ion channel is opened so that ions can diffuse into it. Our key result below is to give a boundary-valued partial differential equation for the mean first passage time for an ion to cross the ion channel—this immediately yields an equation for the ion channel current.

Let $\tau_{\mathcal{R}_1, \mathcal{R}_2}^{(\theta, \lambda)}$ denote the mean first passage time for any of the $N/2$ K^+ ions in \mathcal{R}_1 to travel to \mathcal{R}_2 via the channel \mathcal{C} , and $\tau_{\mathcal{R}_2, \mathcal{R}_1}^{(\theta, \lambda)}$ denote the mean first passage time for any of the $N/2$ K^+ ions in \mathcal{R}_2 to travel to \mathcal{R}_1 :

$$\begin{aligned} \tau_{\mathcal{R}_1, \mathcal{R}_2}^{(\theta, \lambda)} &= \mathbf{E}\{t_{\beta}\} \text{ where } t_{\beta} \equiv \inf \left\{ t : \max \left(z_t^{(1)}, z_t^{(2)}, \dots, z_t^{(N/2)} \right) \geq \beta \right\}, \\ \tau_{\mathcal{R}_2, \mathcal{R}_1}^{(\theta, \lambda)} &= \mathbf{E}\{t_{\alpha}\} \text{ where } t_{\alpha} \equiv \inf \left\{ t : \min \left(z_t^{(N/2+1)}, z_t^{(N/2+2)}, \dots, z_t^{(2N)} \right) \leq \alpha \right\}. \end{aligned} \quad (15.22)$$

In cationic channels, for example, only K^+ or Na^+ ions flow through to cause the channel current—so we do not need to consider the mean first passage time of the

15. Brownian Dynamics

Cl^- ions. To give a partial differential equation for $\tau_{\mathcal{R}_1, \mathcal{R}_2}^{(\theta, \lambda)}$ and $\tau_{\mathcal{R}_2, \mathcal{R}_1}^{(\theta, \lambda)}$, it is convenient to define the closed sets

$$\begin{aligned}\mathcal{P}_2 &= \left\{ \zeta : \{z^{(1)} \geq \beta\} \cup \{z^{(2)} \geq \beta\} \cup \dots \cup \{z^{(N/2)} \geq \beta\} \right\} \\ \mathcal{P}_1 &= \left\{ \zeta : \{z^{(N/2+1)} \leq \alpha\} \cup \{z^{(N/2+2)} \leq \alpha\} \cup \dots \cup \{z^{(2N)} \leq \alpha\} \right\}.\end{aligned}\quad (15.23)$$

Then it is clear that $\zeta_t \in \mathcal{P}_2$ is equivalent to $\max(z_t^{(1)}, z_t^{(2)}, \dots, z_t^{(N/2)}) \geq \beta$ since either expression implies that at least one ion has crossed from \mathcal{R}_1 to \mathcal{R}_2 . Similarly, $\zeta_t \in \mathcal{P}_1$ is equivalent to $\min(z_t^{(N/2+1)}, z_t^{(N/2+2)}, \dots, z_t^{(2N)}) \leq \alpha$. Thus, t_β and t_α defined in Eq. 15.22 can be expressed as $t_\beta = \inf\{t : \zeta_t \in \mathcal{P}_2\}$, $t_\alpha = \inf\{t : \zeta_t \in \mathcal{P}_1\}$.

In a typical ionic channel, $\tau_{\mathcal{R}_2, \mathcal{R}_1}^{(\theta, \lambda)}$ is much larger compared to $\tau_{\mathcal{R}_1, \mathcal{R}_2}^{(\theta, \lambda)}$. In terms of the mean passage rate $\tau_{\mathcal{R}_2, \mathcal{R}_1}^{(\theta, \lambda)}$, $\tau_{\mathcal{R}_1, \mathcal{R}_2}^{(\theta, \lambda)}$, the mean current flowing from \mathcal{R}_1 via the ion channel \mathcal{C} into \mathcal{R}_2 is defined as

$$I^{(\theta, \lambda)} = q^+ \left(\frac{1}{\tau_{\mathcal{R}_1, \mathcal{R}_2}^{(\theta, \lambda)}} - \frac{1}{\tau_{\mathcal{R}_2, \mathcal{R}_1}^{(\theta, \lambda)}} \right). \quad (15.24)$$

The following result, adapted from Gihman and Skorohod (1972, pp. 306) shows that the mean passage times $\tau_{\mathcal{R}_1, \mathcal{R}_2}^{(\theta, \lambda)}$, $\tau_{\mathcal{R}_2, \mathcal{R}_1}^{(\theta, \lambda)}$ satisfy a boundary-valued partial differential equation. In particular, the expressions for the mean first passage time below, together with Eq. 15.24, give a complete characterization of the ion channel current. Of course, the partial differential equation cannot be solved in closed form—so later on in this chapter we use BD simulation as a randomized numerical method for solving this partial differential equation.

Theorem 3. *Consider the two step BD probabilistic construction in Procedure 1. Then the mean passage times $\tau_{\mathcal{R}_1, \mathcal{R}_2}^{(\theta, \lambda)}$ and $\tau_{\mathcal{R}_2, \mathcal{R}_1}^{(\theta, \lambda)}$ (defined in Eq. 15.24) for ions to diffuse through the ion channel are obtained as*

$$\tau_{\mathcal{R}_1, \mathcal{R}_2}^{(\theta, \lambda)} = \int \tau_{\mathcal{R}_1, \mathcal{R}_2}^{(\theta, \lambda)}(\zeta) \pi_\infty^{(\theta, \lambda)}(\zeta) d\zeta \quad (15.25)$$

$$\tau_{\mathcal{R}_2, \mathcal{R}_1}^{(\theta, \lambda)} = \int \tau_{\mathcal{R}_2, \mathcal{R}_1}^{(\theta, \lambda)}(\zeta) \pi_\infty^{(\theta, \lambda)}(\zeta) d\zeta \quad (15.26)$$

where

$$\tau_{\mathcal{R}_1, \mathcal{R}_2}^{(\theta, \lambda)}(\zeta) = \mathbf{E}\{\inf\{t : \zeta_t \in \mathcal{P}_2 | \zeta_0 = \zeta\}\},$$

$$\tau_{\mathcal{R}_2, \mathcal{R}_1}^{(\theta, \lambda)}(\zeta) = \mathbf{E}\{\inf\{t : \zeta_t \in \mathcal{P}_1 | \zeta_0 = \zeta\}\}.$$

Shin-Ho Chung and Vikram Krishnamurthy

Here $\tau_{\mathcal{R}_1, \mathcal{R}_2}^{(\theta, \lambda)}(\zeta)$ and $\tau_{\mathcal{R}_2, \mathcal{R}_1}^{(\theta, \lambda)}(\zeta)$ satisfy the following boundary value partial differential equations:

$$\begin{aligned} \mathcal{L}\tau_{\mathcal{R}_1, \mathcal{R}_2}^{(\theta, \lambda)}(\zeta) &= -1 \quad \zeta \notin \mathcal{P}_2, & \tau_{\mathcal{R}_1, \mathcal{R}_2}^{(\theta, \lambda)}(\zeta) &= 0 \quad \zeta \in \mathcal{P}_2 \\ \mathcal{L}\tau_{\mathcal{R}_2, \mathcal{R}_1}^{(\theta, \lambda)}(\zeta) &= -1 \quad \zeta \notin \mathcal{P}_1, & \tau_{\mathcal{R}_2, \mathcal{R}_1}^{(\theta, \lambda)}(\zeta) &= 0 \quad \zeta \in \mathcal{P}_1 \end{aligned} \quad (15.27)$$

where \mathcal{L} denotes the backward operator defined in Eq. 15.16.

15.6 Brownian Dynamics Simulation

It is not possible to solve the boundary-valued partial differential equations, given in Eq. 15.27, to obtain explicit closed form expressions. The aim of BD simulation is to obtain estimates of these quantities by directly simulating the stochastic dynamical system Eq. 15.7. Thus, BD simulation can be viewed as a randomized numerical method for solving this partial differential equation.

To implement the BD simulation algorithm described below on a digital computer, it is necessary to discretize the continuous-time dynamical equation of the $2N$ ions Eq. 15.7. A two-time scale time discretization is used in the BD simulation algorithm. For dynamics of ions within the ion channel, The BD simulation algorithm uses a sampling interval of $\Delta = 2 \times 10^{-15}$ s. For dynamics of ions within the reservoirs a sampling interval of $\Delta = 2 \times 10^{-12}$ s is used in the reservoirs. There are several possible methods for time discretization of the stochastic differential equation Eq. 15.7, as described in detail by Kloeden and Platen (1992). Our BD simulation algorithm uses the second-order discretization approximation of van Gunsteren et al. (1981).

In the BD simulation algorithm below, we use the following notation:

The algorithm runs for L iterations where L is user specified. Each iteration l , $l = 1, 2, \dots, L$, runs for a random number of discrete-time steps until an ion crosses the channel. We denote these random times as $\hat{\tau}_{\mathcal{R}_1, \mathcal{R}_2}^{(l)}$ if the ion has crossed from \mathcal{R}_1 to \mathcal{R}_2 and $\hat{\tau}_{\mathcal{R}_2, \mathcal{R}_1}^{(l)}$ if the ion has crossed from \mathcal{R}_2 to \mathcal{R}_1 . Thus

$$\hat{\tau}_{\mathcal{R}_1, \mathcal{R}_2}^{(l)} = \min\{k : \zeta_k^{(d)} \in \mathcal{P}_2\}, \quad \hat{\tau}_{\mathcal{R}_2, \mathcal{R}_1}^{(l)} = \min\{k : \zeta_k^{(d)} \in \mathcal{P}_1\}.$$

The positive ions $\{1, 2, \dots, N/2\}$ are in \mathcal{R}_1 at steady state $\pi_{\infty}^{\theta, \lambda}$, and the positive ions $\{N/2 + 1, \dots, 2N\}$ are in \mathcal{R}_2 at steady state.

$L_{\mathcal{R}_1, \mathcal{R}_2}$ is a counter that counts how many K^+ ions have crossed from \mathcal{R}_1 to \mathcal{R}_2 and $L_{\mathcal{R}_2, \mathcal{R}_1}$ counts how many K^+ ions have crossed from \mathcal{R}_2 to \mathcal{R}_1 . Note

$$L_{\mathcal{R}_1, \mathcal{R}_2} + L_{\mathcal{R}_2, \mathcal{R}_1} = L.$$

15. Brownian Dynamics

In the algorithm below, to simply notation, we only consider passage of K^+ ions $i = 1, \dots, N$ across the ion channel.

Algorithm 1. Brownian dynamics simulation algorithm for ion permeation (for fixed θ and λ)

- Input parameters θ for PMF and λ for applied external potential.
- For $l = 1$ to L iterations:
 - *Step 1.* Initialize all $2N$ ions according to the stationary distribution $\pi_{\infty}^{(\theta, \lambda)}$ defined in Eq. 15.18.
Open ion channel at discrete time $k = 0$ and set $k = 1$.
 - *Step 2.* Propagate all $2N$ ions according to the time discretized BD system until time k^* at which an ion crosses the channel.
 - * If ion crossed ion channel from \mathcal{R}_1 to \mathcal{R}_2 , i.e., for any ion $i^* \in \{1, 2, \dots, N/2\}$, $z_{k^*}^{(i^*)} \geq \beta$ then set $\hat{\tau}_{\mathcal{R}_1, \mathcal{R}_2}^{(l)} = k^*$.
Update number of crossings from \mathcal{R}_1 to \mathcal{R}_2 : $L_{\mathcal{R}_1, \mathcal{R}_2} = L_{\mathcal{R}_1, \mathcal{R}_2} + 1$.
 - * If ion crossed ion channel from \mathcal{R}_2 to \mathcal{R}_1 , i.e., for any ion $i^* \in \{N/2 + 1, \dots, N\}$, $z_{k^*}^{(i^*)} \leq \alpha$ then set $\hat{\tau}_{\mathcal{R}_2, \mathcal{R}_1}^{(l)} = k^*$.
Update number of crossings from \mathcal{R}_2 to \mathcal{R}_1 : $L_{\mathcal{R}_2, \mathcal{R}_1} = L_{\mathcal{R}_2, \mathcal{R}_1} + 1$.
 - End for loop.
- Compute the mean passage time and mean current estimate after L iterations as

$$\hat{\tau}_{\mathcal{R}_1, \mathcal{R}_2}^{(\theta, \lambda)}(L) = \frac{1}{L_{\mathcal{R}_1, \mathcal{R}_2}} \sum_{l=1}^{L_{\mathcal{R}_1, \mathcal{R}_2}} \hat{\tau}_{\mathcal{R}_1, \mathcal{R}_2}^{(l)}, \quad \hat{\tau}_{\mathcal{R}_2, \mathcal{R}_1}^{(\theta, \lambda)}(L) = \frac{1}{L_{\mathcal{R}_2, \mathcal{R}_1}} \sum_{l=1}^{L_{\mathcal{R}_2, \mathcal{R}_1}} \hat{\tau}_{\mathcal{R}_2, \mathcal{R}_1}^{(l)}. \quad (15.28)$$

$$\hat{I}^{\theta, \lambda}(L) = q^+ \left(\frac{1}{\hat{\tau}_{\mathcal{R}_1, \mathcal{R}_2}^{(\theta, \lambda)}(L)} - \frac{1}{\hat{\tau}_{\mathcal{R}_2, \mathcal{R}_1}^{(\theta, \lambda)}(L)} \right) \quad (15.29)$$

The following result shows that the estimated current $\hat{I}^{(\theta, \lambda)}(L)$ obtained from a BD simulation run over L iterations is strongly consistent. This means that if the BD simulation is run for a large number of iterations, i.e., as $L \rightarrow \infty$, the estimate of the current obtained from the BD simulation converges with probability one (w.p.1) to the actual ion channel current that was theoretically obtained in Eq. 15.24 in terms of mean passage rates. Thus, this theorem shows that BD simulation is a statistically valid algorithm for estimating the ion channel current.

Theorem 4. For fixed PMF $\theta \in \Theta$ and applied external potential $\lambda \in \Lambda$, the channel current estimate $\hat{I}^{\theta, \lambda}(L)$ obtained from the BD simulation Algorithm 1 over L iterations is strongly consistent, that is,

$$\lim_{L \rightarrow \infty} \hat{I}^{\theta, \lambda}(L) = I^{(\theta, \lambda)} \quad \text{w.p.1} \quad (15.30)$$

Shin-Ho Chung and Vikram Krishnamurthy

where $I^{(\theta, \lambda)}$ is the mean current defined in Eq. 15.24.

Proof. Since by construction in Algorithm 1, each of the L iterations are statistically independent, and $\mathbf{E}\{\hat{\tau}_{\mathcal{R}_1, \mathcal{R}_2}^{(l)}\}$, $\mathbf{E}\{\hat{\tau}_{\mathcal{R}_2, \mathcal{R}_1}^{(l)}\}$ are finite, it then follows by Kolmogorov's strong law of large numbers (Billingsley, 1986)

$$\lim_{L \rightarrow \infty} \hat{\tau}_{\mathcal{R}_1, \mathcal{R}_2}^{(\theta, \lambda)}(L) = \tau_{\mathcal{R}_1, \mathcal{R}_2}^{(\theta, \lambda)}, \quad \lim_{L \rightarrow \infty} \hat{\tau}_{\mathcal{R}_2, \mathcal{R}_1}^{(\theta, \lambda)}(L) = \tau_{\mathcal{R}_2, \mathcal{R}_1}^{(\theta, \lambda)} \quad \text{w.p.1.}$$

Thus, $q^+ \left(\frac{1}{\tau_{\mathcal{R}_1, \mathcal{R}_2}^{(\theta, \lambda)}(L)} - \frac{1}{\tau_{\mathcal{R}_2, \mathcal{R}_1}^{(\theta, \lambda)}(L)} \right) \rightarrow I^{(\theta, \lambda)}$ w.p.1 as $L \rightarrow \infty$.

15.7 Adaptive Controlled Brownian Dynamics Simulation

In this section, we briefly describe a new extension of BD simulation for estimating the PMF of an ion channel. This extension involves a novel simulation-based learning control algorithm that dynamically adapts the evolution of the BD simulation. It is based on our current and on-going research. The complete formalism, convergence proofs, and numerical results will be presented elsewhere (Krishnamurthy and Chung, 2005).

We estimate the PMF U_θ parameterized by some finite-dimensional parameter θ (e.g., θ are the means, variances, and mixture weights of a Gaussian basis function approximation), by computing the parameter θ that optimizes the fit between the mean current $I(\theta, \lambda)$ (defined above in Eq. 15.24) and the experimentally observed current $y(\lambda)$ defined below. There are two reasons why estimating the PMF U_θ is useful. First, by directly estimating PMF, the need for solving Poisson's equation is obviated. Thus, the problem of assigning the effective dielectric constants of the pore and of the protein is avoided. Second, no assumption about the ionization state of some of the residues lining the pore has to be made.

Unfortunately, it is impossible to explicitly compute $I(\theta, \lambda)$ from Eq. 15.24. For this reason we resort to a *stochastic optimization problem formulation* below, where consistent estimates of $I(\theta, \lambda)$ are obtained via the BD simulation algorithm.

From experimental data, an accurate estimate of the current–voltage–concentration profiles of an ion channel can be obtained. These curves depict the actual current $y(\lambda)$ flowing through an ion channel for various external applied potentials $\lambda \in \Lambda$ and ionic concentrations. For a fixed applied field $\lambda \in \Lambda$ at a given concentration, define the square error loss function as

$$\mathcal{Q}(\theta, \lambda) = \mathbf{E} \left\{ \hat{I}_n(\theta, \lambda) - y(\lambda) \right\}^2, \quad \mathcal{Q}(\theta) = \sum_{\lambda \in \Lambda} \mathcal{Q}(\theta, \lambda). \quad (15.31)$$

Note that the total loss function $\mathcal{Q}(\theta)$ is obtained by adding the square error over all the applied fields $\lambda \in \Lambda$ on the current–voltage or current–concentration

15. Brownian Dynamics

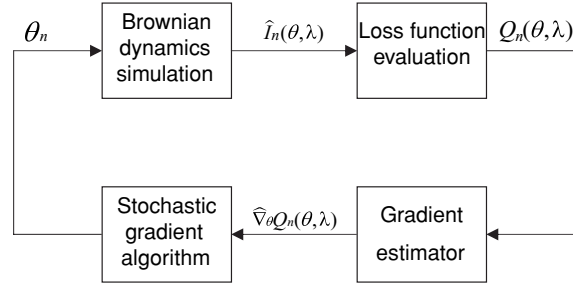


Fig. 15.7 Block diagram of controlled Brownian dynamics simulations for estimating PMF. The currents obtained from Brownian dynamics simulations using the parameters of the initial PMF are compared with the experimental measurements. The parameters for the next iteration is modified such that it would reduce the difference between the simulated and experimental results. The procedure is iterated many times.

curve. The optimal PMF U_{θ^*} is determined by the parameter θ^* that best fits the mean current $I(\theta, \lambda)$ to the experimentally determined curves of an ion channel, i.e.,

$$\theta^* = \arg \min_{\theta \in \Theta} Q(\theta) \quad (15.32)$$

Suppose that the BD simulation Algorithm is run in batches indexed by batch number $n = 1, 2, \dots$. In each batch n , the PMF parameter θ_n is selected (as described below), the BD Algorithm is run over L iterations, and the estimated current $\hat{I}_n(\theta, \lambda)$ is computed using (Eq. 15.29). In summary, Eqs. 15.32 and 15.31 define the stochastic optimization problem we will solve in this section.

To solve the stochastic optimization problem by a simulation-based optimization approach, we need to evaluate unbiased estimates $Q_n(\theta, \lambda)$ of the loss function and derivative estimates $\hat{\nabla}_{\theta} Q_n(\theta, \lambda)$. The estimation of the derivative $\hat{\nabla}_{\theta} Q_n(\theta, \lambda)$ involves using recent sophisticated techniques in Monte-Carlo gradient estimation (see, Vazquez and Krishnamurthy, 2003). Krishnamurthy and Chung (2005) present several such algorithms including the Kiefer–Wolfowitz algorithm which evaluates derivative estimates as finite differences, simultaneous perturbation stochastic approximation (SPSA) which evaluates the derivatives in random directions (and thus saves computational cost), and pathwise infinitesimal perturbation analysis (IPA) gradient estimators.

The controlled BD simulation algorithm for estimating the PMF is schematically depicted in Fig. 15.7. Using an initial parameter set θ , several BD simulations are carried out under various applied potentials and concentrations. From the results of these simulations, the loss function for each BD simulation is computed, using Eq. 15.31. From the total loss function, a new parameter set θ is estimated, based on a stochastic gradient algorithm, and the entire process is repeated. The iterative algorithm for carrying out controlled BD simulation is summarized below.


Shin-Ho Chung and Vikram Krishnamurthy

- *Step 0*: Set batch index $n = 0$, and initialize $\theta_0 \in \Theta$.
- *Step 1 (Evaluation of loss function)*: At batch n , evaluate loss function $\mathcal{Q}_n(\theta_n, \lambda)$ for each external potential $\lambda \in \Lambda$.
- *Step 2 (Gradient estimation)*: Compute gradient estimate $\widehat{\nabla}_{\theta} \mathcal{Q}_n(\theta, \lambda)[\theta_n]$.
- *Step 3 (Stochastic approximation Algorithm)*: Update PMF estimate:

$$\theta_{n+1} = \theta_n - \epsilon_{n+1} \sum_{\lambda \in \Lambda} \widehat{\nabla}_{\theta} \mathcal{Q}_n(\theta_n, \lambda), \quad (15.33)$$

where $\epsilon_n = 1/n$ denotes a decreasing step size.

- Set n to $n + 1$ and go to Step 1.

A crucial aspect of the above algorithm is the gradient estimation Step 2. In this step, an estimate $\widehat{\nabla}_{\theta} \mathcal{Q}_n(\theta, \lambda)$ of the gradient $\nabla_{\theta} \mathcal{Q}_n(\theta, \lambda)$ is computed. This gradient estimate is then fed to the stochastic gradient algorithm (Step 3) which updates the PMF. It can be proved via standard arguments in stochastic approximations that the above algorithm converges to the optimal PMF θ^* w.p.1 

15.8 Concluding Remarks

Three computational tools discussed in this volume—Poisson–Nernst–Planck theory (Coalson and Kurnikova, 2006), molecular dynamics (Grottesi et al., 2006), and Brownian dynamics—will play increasingly prominent roles in understanding how biological ion channel work. Each of these approaches has its strengths and limitations, and involves a degree of approximation. The main defects of Poisson–Nernst–Planck theory are errors stemming from the mean-field assumption. In particular, it ignores the effects of induced surface charges created as a charged particle in electrolyte solutions approaches the protein boundary. The magnitude of the errors introduced by the mean-field approximation become large when the theory is applied to a narrow ionic channels. By incorporating a term in the PNP equations to account for the barrier created by induced surface charges, the magnitude of the errors can be reduced somewhat (Corry et al., 2003). However, doing this removes much of the simplicity of the theory, one of its main advantages over the other approaches, and also it is still hard to know the accuracy of the results without comparison to a more detailed model.

The greatest limitations of molecular dynamics is the computational power required that limits the possible simulation times. While the calculation of free energy profiles provides useful information on ion permeation, it is not a substitute for a direct estimation of conductance from simulations. Thus, virtually no predictions derived from molecular dynamics simulations can be directly compared with experimental data. If no such comparisons can be made, there can only be a limited interaction between experimenters and theoreticians. With the current doubling of computer speeds every 2 years, this computational limitation will eventually be

15. Brownian Dynamics

overcome. Then, the force fields employed in molecular dynamics simulations may need to be improved to include polarization effects, perhaps using *ab initio* molecular dynamics as a guide.

One of the main caveats to the application of Brownian dynamics to biological ion channels is the use of Poisson's equation to estimate the forces encountered by permeant ions. The issue here is whether one can legitimately employ macroscopic electrostatics in regions that are not much larger than the diameters of the water molecules and ions. In the narrow constricted region of the channel, such as in the selectivity filter of the potassium channel, the representation of the channel contents as a continuous medium is a poor approximation.

All three theoretical approaches are useful in elucidating the mechanisms underlying selectivity and permeation of ions across biological nanotubes. For ion channels with large pore radii, such as mechanosensitive channels, Poisson–Nernst–Planck theory can be fruitfully utilized. Also, if one is interested in simply obtaining order-of-magnitude estimates of conductances of various model channels, this simple theory will provide the answers with little computational cost. To study the mechanisms underlying the selectivity sequences of monovalent ions or to determine the precise conformational changes of the protein when a channel undergoes the transition from the closed to the open state, one has to rely on molecular dynamics simulations.

The ability to compute current flow across ion channels confers a distinct advantage to Brownian dynamics compared to molecular dynamics. Because ions are treated as discrete entities, induced surface charges are correctly accounted for. Thus, an obvious application of Brownian dynamics is the calculation of current–voltage and conductance–concentration curves, which can be directly compared to the physiological measurements to assess the reliability and predictive power of the method. In addition to simple counting of ions crossing the channel, one can carry out a trajectory analysis of ions in the system to determine their average concentrations and the steps involved in conduction. This is useful in finding the binding sites and the average number of ions in the channel, both of which are experimentally observable quantities. It is also possible to study the mechanisms of blocking of channels by larger molecules or other ion species.

Brownian dynamics has been extensively used in the past to simulate the current flowing across a variety of model ion channels (Allen et al., 1999, 2000; Allen and Chung, 2001; Chung et al., 1999, 2002a, b; Corry et al., 2001, 2004a, b; Im and Roux, 2002a, b; Noskov et al., 2004; O'Mara et al., 2003, 2005; Vora et al., 2004). Here we show that BD simulation is a statistically valid algorithm for estimating the ion channel current, placing this nonequilibrium method used by the previous authors in studying model ion channels on a firm mathematical foundation. In BD, the propagation of ions in the ion channel is modeled as a large-scale, multi-particle continuous-time, stochastic dynamical system satisfying the Langevin equation. The key idea here is that instead of considering the dynamics of individual water molecules, which is computationally intractable, the BD system considers the average effect of water molecules as a random force acting on individual ions. This

Au: The year
"2001" here
has been
changed into
"2000". Is this
OK?



Shin-Ho Chung and Vikram Krishnamurthy

treatment of water molecules can be viewed as an approximation of the central-limit theorem by using stochastic averaging of water molecules. We then provide the proof that ions drifting executing Brownian motion in a simulation assembly in which a channel protein is imbedded achieve a stationary distribution (steady state) exponentially fast (Theorem 1). We also demonstrate that the current across the model pore is related to the mean first passage time of ions, which satisfies a boundary-valued partial differential equation related to the Fokker–Planck equation. Thus, BD can be construed as a randomized algorithm for numerically solving this partial differential equation. The simulated current converges to the explicit solution of the partial differential equation w.p.1 (Theorem 4).

The mathematical formulation and statistical analysis of BD we provide in this chapter are essential for further extension and refinement of the method. With the BD method placed on a firm theoretical ground, we are now in the position to further refine and extend it by applying the state-of-the-art, novel stochastic estimation algorithms, thus making this approach far more versatile than in its current form. One of the major caveats to the use of BD in studying the permeation dynamics in biological ion channels is the use of Poisson’s equation to calculate the forces encountered by permeant ions. The issue here is whether one can legitimately employ macroscopic electrostatics in regions that are not much larger than the diameters of the water molecules and ions. In the narrow, constricted region of the channel, such as in the selectivity filter of the potassium channel, the representation of the channel contents as a continuous medium is a poor approximation. The method of adaptive controlled BD, which we discussed briefly, is designed to circumvent the limitations posed in the conventional simulation approach. Using the learning-based dynamic control algorithm, we are able to solve the inverse problem. That is, given the three-dimensional shape of a channel, we can deduce the potential of mean force encountered by an ion traversing the channel that correctly replicates experimental findings, thus obviating the need to solve Poisson’s equation. The BD algorithm thus can now be used to study the propagation of individual ions through a mesoscopic system where continuum electrostatics breaks down (Edwards et al., 2002) and molecular dynamics fails to yield a sensible profile of the PMF (Allen et al., 2003, 2004). Alternatively, if continuum electrostatic is to be applied, we can pinpoint, using a stationary stochastic optimization algorithm, the effective dielectric constants of the pore and of protein that need to be used to replicate experimental measurements.

The combined techniques of statistical signal processing and stochastic control of large-scale dynamic systems of interacting particles will help us unravel the structure–function relationships in ion channels. Also, by combining the state-of-the-art dynamic control algorithms with BD, it should be possible to predict the open-state structure of an ion channel with a fair degree of certainty and also design new nanotubes that can be utilized as antifungal or antibacterial agents. Now and in the near future, as we attempt to understand membrane channels in terms of rigorous molecular physics, there will be an increasing interplay between experiment and

15. Brownian Dynamics

theory, the former providing hints and clues for building and refining models and the later making testable predictions.

References

- Accardi, A., and C. Miller. 2004. Secondary active transport mediated by a prokaryotic homologue of ClC Cl⁻ channels. *Nature* 427:803–807.
- Allen, T.W., O.S. Andersen, and B. Roux. 2004. On the importance of atomic fluctuations, protein flexibility, and solvent in ion permeation. *J. Gen. Physiol.* 124:679–690.
- Allen, T.W., T. Bastug, S. Kuyucak, and S.H. Chung. 2003. Gramicidin A channel as a test ground for molecular dynamics force fields. *Biophys. J.* 84:2159–2168.
- Allen, T.W., and S.H. Chung. 2001. Brownian dynamics study of an open-state KcsA potassium channel. *Biochim. Biophys. Acta Biomembr.* 1515:83–91.
- Allen, T.W., M. Hoyles, S. Kuyucak, and S.H. Chung. 1999. Molecular and Brownian dynamics study of ion permeation across the potassium channel. *Chem. Phys. Letts.* 313:358–365.
- Allen, T.W., S. Kuyucak, and S.H. Chung. 2000. Molecular dynamics estimates of ion diffusion in model hydrophobic and KcsA potassium channels. *Biophys. Chem.* 86:1–14.
- Bass, R.B., P. Strope, M. Baraclay, and D.C. Reece. 2002. Crystal structure of *Escherichia coli* MscS, a voltage-modulated and mechanosensitive channel. *Science* 298:1582–1587.
- Bek, S., and E. Jakobsson. 1994. Brownian dynamics study of a multiply occupied cation channels: Application to understanding permeation in potassium channel. *Biophys. J.* 66:1028–1038.
- Billingsley, P. 1986. Probability and Measure. Wiley, New York.
- Burykin, A., C.N. Schutz, J. Villa, and A. Warshel. 2002. Simulations of ion current realistic models of ion channels: KcsA potassium channel. *Proteins Struct. Funct. Genet.* 47:265–280.
- Chang, G., R.H. Spencer, A.T. Lee, M.T. Barclay, and D.C. Rees. 1998. Structure of the ~~mscL~~ homolog from mycobacterium tuberculosis: A gated mechanosensitive channel. *Science* 282:2220–2226.
- Chung, S.H., T.W. Allen, M. Hoyles, and S. Kuyucak. 1999. Permeation of ions across the potassium channel: Brownian dynamics studies. *Biophys. J.* 77:2517–2533.
- Chung, S.H., T.W. Allen, and S. Kuyucak. 2002a. Conducting-state properties of the KcsA potassium channel from molecular and Brownian dynamics simulations. *Biophys. J.* 82:628–645.
- Chung, S.H., T.W. Allen, and S. Kuyucak. 2002b. Modeling diverse range of potassium channels with Brownian dynamics. *Biophys. J.* 83:263–277.
- Chung, S.H., and S. Kuyucak. 2002. Recent advances in ion channel research. *Biochim. Biophys. Acta Biomembr.* 1565:267–286.



Au: Please cite Chung et al. (1998) in the text.

Shin-Ho Chung and Vikram Krishnamurthy

- Chung, S.H., M. Hoyles, T.W. Allen, and S. Kuyucak. 1998. Study of ionic currents across a model membrane channel using Brownian dynamics. *Biophys. J.* 75:793–809.
- Coalson, R., and M.G. Kurnikova. 2005. Poisson–Nernst–Planck theory approach to the calculation of current through biological ion channels. *IEEE Trans. Nanobiosci.* 4:81–93.
- Coalson, R., and M.G. Kurnikova. 2006. Poisson–Nernst–Planck theory of ion permeation through biological channels. In: ~~Handbook of~~ Ion Channels: Dynamics, Structure and Application, S.H. Chung, O.S. Andersen, and V. Krishnamurthy, editors. Springer-Verlag, New York.
- Cooper, K.E., E. Jakobsson, and P. Wolynes. 1985. The theory of ion transport through membrane channels. *Prog. Biophys. Mol. Biol.* 46:51–96.
- Coronado, R., R.L. Rosenberg, and C. Miller. 1980. Ionic selectivity, saturation, and block in a K^+ -selective channel from sarcoplasmic reticulum. *J. Gen. Physiol.* 76:425–446.
- Corry, B., T.W. Allen, S. Kuyucak, and S.H. Chung. 2001. Mechanisms of permeation and selectivity in calcium channels. *Biophys. J.* 80:195–214.
- Corry, B., S. Kuyucak, and S.H. Chung. 2003. Dielectric self-energy in Poisson–Boltzmann and Poisson–Nernst–Planck models of ion channels. *Biophys. J.* 84:3594–3606.
- Corry, B., M. O’Mara, and S.H. Chung. 2004a. Permeation dynamics of chloride ions in the ClC-0 and ClC-1 channels. *Chem. Phys. Lett.* 386:233–238.
- Corry, B., M. O’Mara, and S.H. Chung. 2004b. conduction mechanisms of chloride ions in ClC-type channels. *Biophys. J.* 86:846–860.
- Cuello, L.G., J.G. Romero, D.M. Cortes, and E. Perozo. 1998. pH dependent gating in the *Streptomyces lividans* K^+ channel. *Biochemistry* 37:3229–3236.
- Doyle, D.A., J.M. Cabral, R.A. Pfuetzner, A. Kuo, J.M. Gulbis, S.L. Cohn, B.T. Chait, and R. MacKinnon. 1998. The structure of the potassium channel: Molecular basis of K^+ conduction and selectivity. *Science* 280:69–77.
- Dutzler, R., E.B. Campbell, M. Cadene, B.T. Chait, and R. MacKinnon. 2002. X-ray structure of a ClC chloride channel at 3.0 Å reveals the molecular basis of anion selectivity. *Nature* 415:287–294.
- Dutzler, R., E.B. Campbell, and R. MacKinnon. 2003. Gating the selectivity in ClC chloride channels. *Science* 300:108–112.
- Edwards, S., B. Corry, S. Kuyucak, and S.H. Chung. 2002. Continuum electrostatics fails to describe ion permeation in the gramicidin channel. *Biophys. J.* 83:1348–1360.
- Eisenberg, R. S. 1999. From structure to function in open ionic channels. *J. Membr. Biol.* 171:1–24.
- Fahlke, C. 2001. Ion permeation and selectivity in ClC-type chloride channels. *Am. J. Renal Physiol.* 280:F748–F758.
- Garofoli, S., and P.C. Jordan. 2003. Modeling permeation energetics in the KcsA potassium channel. *Biophys. J.* 84:2814–2830.

15. Brownian Dynamics

- Gihman, I., and A. Skorohod. 1972. Stochastic Differential Equations. Springer-Verlag, Berlin.
- Grottesi, A., C. Domene, S. Haider, and M.S.P. Sansom. 2005. Molecular dynamics simulation approaches to K channels: Conformational flexibility and physiological function. *IEEE Trans. Nanobiosci.* 4:112–120.
- Grottesi, A., S. Haider, and M.S.P. Sansom. 2006. Molecular dynamics simulation approaches to K channels. In: *Handbook of Ion Channels: Dynamics, Structure and Application*, S.H. Chung, O.S. Andersen, and V. Krishnamurthy, editors. Springer-Verlag, New York.
- Guàrdia, E., R. Rey, and J. Padró. 1991a. $\text{Na}^+ - \text{Na}^+$ and $\text{Cl}^- - \text{Cl}^-$ ion pairs in water: Mean force potentials by constrained molecular dynamics. *J. Chem. Phys.* 95:2823–2831.
- Guàrdia, E., R. Rey, and J. Padró. 1991b. Potential of mean force by constrained molecular dynamics: A sodium chloride ion-pair in water. *J. Chem. Phys.* 155:187–195.
- Heginbotham, L., M. LeMasurier, L. Kolmakova-Partensky, and C. Miller. 1999. Single *Streptomyces lividans* K^+ channels: Functional asymmetries and sidedness of proton activation. *J. Gen. Physiol.* 114:551–559.
- Hille, B. 2001. Ionic Channels of Excitable Membranes, 3rd Ed. Sinauer Associates, Sunderland, MA.
- Im, W., and B. Roux. 2002a. Ion permeation and selectivity of ompf porin: A theoretical study based on molecular dynamics, Brownian dynamics, and continuum electrodiffusion theory. *J. Mole. Biol.* 322:851–869.
- Im, W., and B. Roux. 2002b. Ions and counterions in a biological channel: A molecular dynamics simulation of ompf porin from *Escherichia coli* in an explicit membrane with 1 M KCl aqueous salt solution. *J. Mol. Biol.* 319:1177–1197.
- Jakobsson, E., and W.W. Chiu. 1987. Stochastic theory of singly occupied ion channels. *Biophys. J.* 52:33–45.
- Jentsch, T.J., T. Friedrich, A. Schriever, and H. Yamada. 1999. The ClC chloride channel family. *Pflügers Arch.* 437:783–795.
- Jordan, P.C. 1999. Ion permeation and chemical kinetics. *J. Gen. Physiol.* 114:601–604.
- Jordan, P.C. 2005. Semimicroscopic modeling of permeation energetics in ion channels. *IEEE Trans. Nanobiosci.* 4:94–101.
- Jordan, P.C. 2006. A mesoscopic-microscopic perspective on ion channel permeation energetics: The semi-microscopic approach. In: *Handbook of Ion Channels: Dynamics, Structure and Application*, S.H. Chung, O.S. Andersen, and V. Krishnamurthy, editors. Springer-Verlag, New York.
- Karatzas, I., and S.E. Shreve. 1991. Brownian Motion and Stochastic Calculus. Springer-Verlag, New York.
- Kloeden, P.E., and E. Platen. 1992. Numerical Solution of Stochastic Differential Calculus. Springer-Verlag, Berlin.

Shin-Ho Chung and Vikram Krishnamurthy

- Krishnamurthy, V., and S.H. Chung. 2005. Brownian dynamics simulation for modeling ion permeation across bio-nanotubes. *IEEE Trans. Nanobiosci.* 4:102–111.
- LeMasurier, M., L. Heginbotham, and C. Miller. 2001. KcsA: It's a potassium channel. *J. Gen. Physiol.* 118:303–313.
- Long, S.B., E.B. Campbell, and R. MacKinnon. 2004a. Crystal structure of a mammalian voltage-dependent *Shaker* family K⁺ channel. *Science* 309:897–903.
- Long, S.B., E.B. Campbell, and R. MacKinnon. 2004b. Voltage sensor of Kv1.2: Structural basis of electromechanical coupling. *Science* 309:903–908.
- Maduke, M., C. Miller, and J.A. Mindell. 2000. A decade of ClC chloride channels: Structure, mechanism, and many unsettled questions. *Annu. Rev. Biophys. Biomol. Struct.* 29:411–438.
- Mashl, R.J., Y. Tang, J. Schnitzer, and E. Jakobsson. 2001. Hierarchical approach to predicting permeation in ion channels. *Biophys. J.* 81:2473–2483.
- McCleskey, E.M. 1999. Calcium channel permeation: A field in flux. *J. Gen. Physiol.* 113:765–772.
- Meuser, D., H. Splitt, R. Wagner, and H. Schrempf. 1999. Explorign the open pore of the potassium channel from *Streptomyces lividans*. *FEBS Letts.* 462:447–452.
- Miller, C. 1982. Open-state substructure of single chloride channels from *torpedo electroplax*. *Phil. Trans. R. Soc. Lond. B* 299:401–411.
- Noskov, S.Yu., S. Bernéche, and B. Roux. 2004. Control of ion selectivity in potassium channels by electrostatic and dynamic properties of carbonyl ligands. *Nature* 431:830–834.
- O'Mara, M., P.H. Barry, and S.H. Chung. 2003. A model of the glycine receptor deduced from Brownian dynamics studies. *Proc. Natl. Acad. Sci. USA* 100:4310–4315.
- O'Mara, M., B. Cromer, M. Parker, and S.H. Chung. 2005. Homology model of GABA_A channel examined with Brownian dynamics. *Biophys. J.* 88:3286–3299.
- Partenskii, M.B., and P.C. Jordan. 1992. Theoretical perspectives on ion-channel electrostatics: Continuum and microscopic approaches. *Q. Rev. Biophys.* 25:477–510.
- Pitera, J.W., M. Falt, and W.F. van Gunsteren. 2001. Dielectric properties of proteins from simulation: The effects of solvent, ligands, pH, and temperature. *Biophys. J.* 80:2546–2555.
- Roux, R., S. Bernéche, and W. Im. 2000. Ion channels, permeation, and electrostatics: Insight into the function of KcsA. *Biochemistry* 39:13295–13306.
- Sanders, J.A., and F. Verhulst. 1985. Averaging Methods in Nonlinear Dynamical Systems. Springer-Verlag, Berlin.
- Schrempf, H., O. Schmidt, R. Kümerlen, S. Hinnah, D. Müller, M. Betzler, T. Steinkamp, and R. Wagner. 1995. A prokaryotic potassium ion channel with two predicted transmembrane segment from *Streptomyces lividans*. *EMBO J.* 14:5170–5178.
- Schutz, C.N., and A. Warshel. 2001. What are the dielectric “constants” of proteins and how to validate electrostatic model. *Proteins* 44:400–417.



15. Brownian Dynamics

- Simonson, T., and C.L. Brooks III. 1996. Charge screening and the dielectric constant of proteins: Insights from molecular dynamics. *J. Am. Chem. Soc.* 118:8452–8458.
- Smith, P.E., R.M. Brunne, A.E. Mark, and W.F. van Gunsteren. 1993. Dielectric properties of trypsin inhibitor and lysozyme calculated from molecular dynamics simulations. *J. Phys. Chem.* 97:2009–2014.
- Stillinger, F.H., and A. Rahman. 1974. Improved simulation of liquid water by molecular dynamics. *J. Chem. Phys.* 60:1545–1557.
- Tieleman, D.P., P.C. Biggin, G.R. Smith, and M.S.P. Sansom. 2001. Simulation approaches to ion channel structure-function relationships. *Q. Rev. Biophys.* 34:473–561.
- Unwin, N. 2005. Refined structure of the nicotinic acetylcholine receptor at 4 Å resolution. *J. Mol. Biol.* 346:967–989.
- van Gunsteren, W., H. Berendsen, and J. Rullman. 1981. Stochastic dynamics for molecules with constraints Brownian dynamics of n-alkalines. *Mol. Phys.* 44:69–95.
- Vazquez, F.J., and V. Krishnamurthy. 2003. Implementation of gradient estimation to a constrained Markov decision problem. In: Proceedings of 42nd IEEE Conference on Decision and Control, pp. 4841–4846.
- Vora, T., B. Corry, and S.H. Chung. 2004. A model of sodium channels. *Biochim. Biophys. Acta Biomembr.* 1668:106–116.
- Wong, E., and B. Hajek. 1985. Stochastic Processes in Engineering System, 2nd Ed. Springer-Verlag, Berlin.

